Supervisory Control Interface for Experimental Hybrid Wind & Solar Energy System

By
Vinod Bachhao

A Thesis Submitted to Saint Mary's University, Halifax, Nova Scotia in Partial Fulfillment of the Requirements for the Degree of Master of Science in Applied Science

April 19, 2018, Halifax, Nova Scotia

Approved: Dr. Adel Merabet
Supervisor
Division of Engineering

Approved: Dr. Jason Rhinelander
Supervisory Committee
Division of Engineering

Approved: Dr. Bashir Khan
Supervisory Committee
Department of Mathematics and Computing Science

Approved: Dr. Zheng Qin
External Examiner
Green Power labs

Date: April 19, 2018

Supervisory Control Interface for Experimental Hybrid Wind & Solar Energy System

By

Vinod Bachhao

Abstract

A supervisory control interface developed for wind and solar energy system and its control systems are presented in this thesis. The proposed system consists of a wind turbine, a solar panel and a load bank. A power electronics interface, based on various converters, is used to integrate the renewable energy sources. The main goal of the control interface is to maintain the balance between load demand and power supply. The objective of the proposed power management system is to ensure a proper control and coordination between all the sources and loads of the system. The developed power management system algorithm uses a basic cost function to control the power flow from both the energy sources. The supervisory control interface also gives the user an option to control the load priority from the front panel and provides user feedback in case of low power situations. An experimental setup is designed using the National Instruments equipment and LabVIEW software to test the developed control interface. Experimental results for various conditions are presented to validate the power management system algorithms developed in this work.

April 19th, 2018

Table of Contents

List of Figures

Nomenclature

Wind Energy Conversion

ρ	Air Density
r	Length of The Turbine Blade
v_w	Wind Speed
λ	Ratio of Blade Tip Speed to Wind Speed
ω	Angular Velocity of The Turbine
I	Armature Current
K_b	Back-EMF Constant
V	Generator Voltage
J	Rotor Inertia
B	Viscous-Friction Coefficient
T_t	Turbine Torque
T_{em}	Generator Torque
T_{iref}	Turbine Current Reference
T_i	Turbine Current.

Solar Energy Conversion

I	Solar Cell Output Current
V	Solar Cell Output Voltage
I_L	Light Generated Current
I_0	Dark Saturation Current
q	Charge of an Electron
A	Diode Quality (Ideality) Factor
k	Boltzmann Constant
T	Absolute Temperature
R_S	Series Resistance
R_{SH}	Shunt Resistances

List of Abbreviations

AC	Alternating Current
CPU	Central Processing Unit
DC	Direct Current
DG	Distributed Generation
HES	Hybrid Energy System
IV	Current-Voltage
KWh	Kilowatt-Hour
LED	Light Emitting Diode
MOSFET	Metal-Oxide-Semiconductor Field-Effect Transistor
MPPT	Maximum Power Point Tracking
NI	National Instruments
PI	Proportional Integral
PMS	Power Management System
PV	Photovoltaic
PVECS	Solar Photovoltaic Energy Conversion System
PWM	Pulse Width Modulation

Chapter 1 Introduction

Renewable energy systems play a vital role in harnessing clean energy by converting naturally available energy source i.e. wind, solar, tidal etc. into electricity and hence providing clean energy for domestic and commercial use. Research in clean technology is imperative to Nova Scotia not only because it helps in reducing dependence on fossil fuel, which in turn prevents health and environmental damage, but also because it is a commitment of the province to make a change. According to Nova Scotia's Electricity Plan 2015 – 2040, Phase one is from now to 2020, a period marked by much-needed power rate stability, a more competitive electricity marketplace, and continued reduction in carbon emissions [1]. The second phase is from 2020 and beyond, in this phase province aims to further reduce its carbon footprint and provide clean and greener energy through the innovations and experiences earned in the first phase.

As the investment in renewable energy systems is increasing we have faced with the inherent problem of the solar and wind energy systems i.e. intermittency of the available energy, which in turn induces nonlinearities in the output of these energy systems. As increasingly digital technology is used to control the energy conversion in renewable energy systems, it comes down to the control algorithms of the system to handle the eventual uncertainties in the output. Hence, it becomes imperative to design and study control algorithms which can help in maximizing energy extraction from the renewable energy system and increase the system reliability.

This research work focuses on designing the supervisory control interface for a wind-solar hybrid energy system. Apart from control interface design, power management algorithm development is done to control the power flow in the energy system from the generation source to the load side. This algorithm uses the weather parameters to such as wind speed and irradiance to decide the load demand and prioritizes the load based on the predesigned load priority setting or the user input load priority. This hybrid system will be also useful in developing a control system from the model of the wind turbine and solar PV and practical realization of this developed hybrid system would bridge the gap between theory and practice. It would allow implementation of theories of advanced control by analyzing the major components of a hybrid system and extracting mathematical models needed for the design of a model-based control system.

1.1. Literature review

A brief literature review is done in this section. Since a major part of this research was hardware and software control interface design of the hybrid energy system, following topics are considered for the literature review.

1. Wind energy conversion system
2. The solar photovoltaic energy conversion system
3. Hybrid energy systems

1.1.1. Wind energy control system

The wind energy conversion system (WECS) in all its forms presents a challenge to control the speed at the desired level. A control system, in this case, must maintain the desired voltage level and operate the wind turbine within rated limits to ensure the safety of the WECS, converters and loads. Various converter configurations and control algorithms are used to control the wind turbine to the desired degree. Some of the studies in [2-6] show the control system design based on various algorithms to control the turbine speed and achieve the desired degree of DC-link voltage regulation. Although controlling the speed is of prime important but other parameters in the system also need close attention to deliver the quality power at the consumer end. To achieve this goal, control system modelling needs to recognize the parameters important to maintain the balance and incorporate those in the system design, several studies [7-10] demonstrate this by using higher order control laws to reduce the effect of nonlinear disturbances to the minimum.

As the control of moving parts in the wind turbine energy system is a major focus in the system design it is also important to look at the aspects of power electronics involved in the system, which are important in converting the and inverting the power generated in the system. The studies in [11-12] demonstrate this by using a laboratory size wind turbine with the blower inside a small wind tunnel. The blower fan inside wind tunnel simulates the wind which in turn rotates the wind turbine to generate by through DC generator connected to the turbine. This arrangement along with power electronics give a decent

setup to model the different controllers, which take into consideration various nonlinear disturbances affecting the system.

1.1.2. The solar photovoltaic energy control system

The solar photovoltaic (PV) systems are nowadays widespread and used in many applications due to their little maintenance requirements and friendly environmental characteristics for its null pollution. One of integral parts of Solar PV energy system is a DC-DC converter, converters have the important function of converting incoming power into suitable power at the output terminal. Making sure best converter configuration and intelligent control algorithms are important for making solar PV systems as a viable energy alternative. As these studies [13-16] show the importance of research in this field and recent development in this direction. The power generation from a Photovoltaic (PV) system gets affected as the optimum operating point changes due to the variation in the environmental factors such as temperature, solar insolation, etc. In spite of the fluctuations, to achieve maximum power from solar energy system, maximum power point tracking (MPPT) technique is essential to extract the maximum available power. A detailed review of various MPPT techniques in [17-19] show the recent trends and various MPPT techniques employed in the solar PV systems. These techniques greatly help in the better-optimized system and hence the efficient use of resources.

Solar PV systems consist of three basic parts the PV panel, the power converter and the tracking controller. To make the solar PV system commercially viable, the cost of unit generation of electricity from solar PV system needs to be reduced which, in turn, calls for the development of a low cost, high efficient power conversion systems or schemes for

delivering required electrical power. Hence it is always critical to design the most appropriate power converters and to assess their performance to ensure maximum power capture from solar modules along with impeccable power quality, reliability and efficiency. A major challenge that needs to be addressed by the DC-DC converters is to take the non-linear output characteristic of the solar PV sources which varies with solar insolation and temperature and convert it into the appropriate level of voltage. During recent years, different DC-DC converter topologies have been investigated for their applicability, safety and protection issues in solar PV power generating system [19-21].

As the research in solar PV energy system has widespread traction it is critical for researchers to have access to research equipment to streamline the research focus on implementable technological solutions. As discussed in [22-26] research focus in these cases shows a pathway to develop the real-time controllers and their implementation to achieve the goal of extracting maximum power from the energy system in the real-world application. Further studies mentioned in [27-30] expand on these ideas in the grid-connected systems, which adds to the system complexity but makes systems more reliable. As the distributed generation is increasing, to increase the renewable system reliability more than one source of generation is added to the system. This presents the challenges in the system control either in grid-connected or in the island mode, next chapter expands on the research in this area of hybrid energy systems.

1.1.3. Hybrid energy systems

Solar and wind power systems exhibit changing dynamics, nonlinearities, and uncertainties—challenges that require advanced control strategies to solve effectively. The

use of more efficient control strategies would not only increase the performance of these systems but, would increase the number of operational hours of solar and wind plants and thus reduce the cost per kilowatt-hour (KWh) produced [31]. To use these efficient control strategies digital systems are needed to be integrated into the existing grid i.e. infrastructure investment to make a smart grid of the future.

As the combining of multiple energy generation sources is increasingly seen as the solution to counter the uncertainty in the weather patterns the recent trend shows that this approach has its advantages and challenges as discussed in these review articles [32,33]. It is also interesting to note that the hybrid system with grid-connected is seen as the structure of the grids of the future. These future grids having their own storage and energy generation sources can act as a standalone system as well as send power into the grid, since this is basically a function of the grid but on the small or micro scale in comparison to the utility grid, these types of systems are now referred to as the microgrids. The studies in [34,35] give a glimpse into this new structure of the grid and also provide a solution to manage such system with niche solutions for particular grid configuration.

Microgrids, although was present in its basic form the lack of technological push in the digital domain had made it less glamorous and kept it as only an isolated energy source. With the addition of digital technology and power electronics to the modern grid infrastructure suddenly monitoring and controlling the energy system seems easier than before. Basically, power electronics along with digital control has made the elements of grid smart hence, the smart microgrids are the new reality and future.

To reach the stage of implementable smart microgrids, digital control of the power electronics played a very important role in this regard. Studies in [36-40] are some of the

several approaches to achieving the control of the renewable energy system converters using digital controllers. Although these control methods achieve the local control of the converters, it becomes extremely important to control the overall system along with proper local control of the energy sources individually. This task of controlling the complete system with its multiple sources of generation and storage is aided by the central controller which keeps the track of the power generated and power consumed and acting as the brain of the system providing references to control the system parameters from the central control. This study [41] give the review of the power management techniques applied to achieve the desired power flow control. Several studies in [42-44] give various control algorithms for power management in the hybrid energy system or microgrid. The control method in these research studies also shows the use of new digital controllers capable of achieving higher performance speed than the tradition CPU (central processing unit) structure of digital controllers. Although utility grid delivers the power to the households in the form of AC (alternating current) but most of the modern electronics used by the people need DC power for that equipment. Research topic in [45,46] uses this as the basis to show the power management in the purely DC grid setting. As the world is moving towards the future smart grid, some of the challenges in the implementation of this future grid remain.

Although smart grid is the grid of the future certain bottlenecks discussed in [47] prevent its rapid growth. The reasons for this stall in growth are mainly: technical, regulatory, financial, and stakeholder. The most common technical barriers include problems with technology components, dual-mode switching from grid-connected to island mode, power quality and control, and protection issues. One of the ways to improve the reliability of

renewable energy systems is to have deterministic control of the power electronics. To achieve this control system needs to have better control strategies to control the overall system [48,49].

The smart grid industry is growing as the global push for renewable energy systems becomes stronger and more urgent. The smart grid is the solution to this problem, it will make use of new design concepts and advanced materials in system components like transformers and circuit breakers to improve efficiency, safety and operational performance. Widespread use of power electronic devices will help maximize the performance of existing assets and make the grid more resilient in the event of disruptions. Energy storage technologies will help mitigate demand peaks and allow the grid to integrate more renewable energy power sources. More flexible transmission and distribution systems can accommodate fluctuations in supply, increase efficiency and optimize system operations. Powerful monitoring and control systems will help prevent disruptions before they occur. A smart grid combines all these features, linked by communication technologies.

The smart grid is conceived of as an electric grid that can deliver electricity in a controlled, smart way from points of generation to active consumers [50]. Innovative enabling technologies and systems, such as smart meters, energy controllers, communication systems, decisive to facilitate the coordination of efficiency and demand-response in a smart grid, are described and discussed with reference to real industrial case studies and research projects.

1.2. Objectives, Scope and Contribution

1) To design power electronic circuit interface for wind energy conversion system (WECS) and solar energy conversion system.

2) To fabricate the designed circuit into hardware assembly on the perforated circuit board.

3) To develop a software interface in the LabVIEW to control the power electronic circuit.

4) To develop supervisory control interface to control the load based on the power generation using PMS (power management system) algorithm.

Contribution - This thesis project intends to provide hardware and software design interface for the experimental laboratory-based Solar-Wind hybrid energy system. In this work laboratory size, wind turbine setup from Quanser Inc. and solar panel from Coleman is used to design a hybrid energy system. Other major components of the system are the National instruments digital controller and an in-house developed power electronics interface. Details of the main contribution are presented in chapter 4.

1.3. Outline of the Thesis

Chapter 2 describes the principle of wind energy conversion system (WECS) that includes a brief introduction to the major components of WECS, modelling wind turbine and the

energy conversion system. It describes control schemes for wind turbine and the electrical configuration developed based on the practical setup

Chapter 3 focuses on the development of solar photovoltaic energy conversion system (PVCS) that includes a background on the fundamentals of PVCS, modelling solar cell, module and PV array. It introduces the major components of PVCS, control schemes and the configuration developed in this work.

Chapter 4 focuses on the design and development of power management system developed for this research work. This chapter gives a detailed introduction to the hybrid energy system configuration used and communication between various system components. In the final section, PMS algorithm is explained in detail with both the auto and manual mode operations of the same

Chapter 5 focuses on the hardware components of this system. This chapter briefly introduces the National Instruments' hardware components used to make this system. It further expands on the software interface developed during this thesis work and gives a brief introduction to the power electronics interface used in the hybrid energy system.

Chapter 6 introduces the experimental setup and explains the load side system configuration and presents the results obtained for various experiment cases designed to test the PMS algorithm introduced in chapter 4.

Chapter 7 concludes the thesis with conclusion and suggestions for future work.

Chapter 2 Wind Turbine Energy System

2.1. Introduction

Wind energy conversion systems (WECS) play a major role in extracting power from the abundantly available source i.e. wind. It typically consists of a wind turbine, mechanical gear system (optional drivetrain), electrical generator, power electronic interface and control system components. The major function of WECS is to convert the kinetic energy from the wind to electrical energy and supply the electrical grid or the loads directly. In recent decades, wind energy has become the predominant viable source of renewable energy. Scientists and engineers have gained considerable experience in handling small to large capacity wind generation systems. Following sections describe the wind turbine energy systems used for this research and its control using a wind turbine side buck converter.

2.2. Wind Turbine Modelling and Characteristics

The wind turbine used in this system, manufactured by Quanser Inc., is installed in a wind tunnel. It has five blades and drives a DC (direct current) generator through a gearbox ratio 1:1. The gearbox converts rotation of the horizontal-axis turbine to that of the vertical-axis generator. The generator is connected to the load via a power electronic interface allowing control of the shaft speed and load voltage. Fig. 1 shows the wind turbine used in this

hybrid energy system. The power delivered by the turbine shaft (neglecting losses in the drive train) is given by [12]

$$P_t = 0.5\pi\rho C_p(\lambda)r^2 v_w^3 \tag{2.a}$$

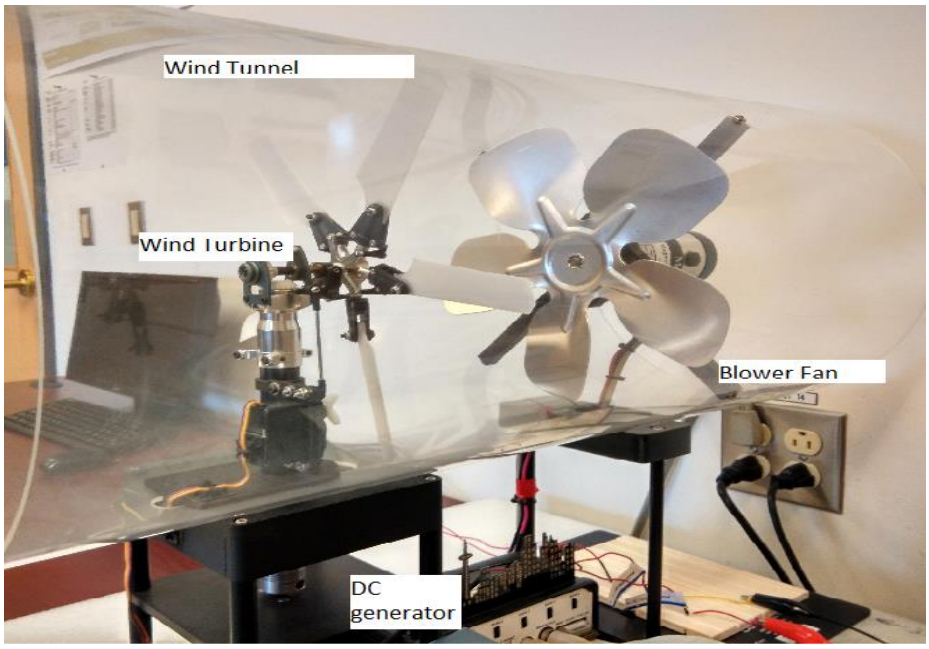

Figure 1 Wind turbine energy system

where ρ denotes the air density, r is the length of the turbine blade, v_w is the wind speed, and λ is the ratio of blade tip speed to wind speed, that is

$$\lambda = \frac{\omega r}{v_w} \tag{2.b}$$

where ω is the angular velocity of the turbine. The power coefficient C_p depends on speeds of the turbine and wind, and its relation to λ shown in Fig. 2. [12]

The power coefficient reaches a maximum at a specific optimum value λ_{opt}. To extract maximum power from wind, the turbine speed should be so controlled as to maintain λ at the optimum level.

In some wind turbines, the optimum tip speed ratio may be unknown or not well defined and subject to change. Therefore, instant locating of the maximum C_p during the operation of wind turbine is very important. An MPPT algorithm is generally used for maximum

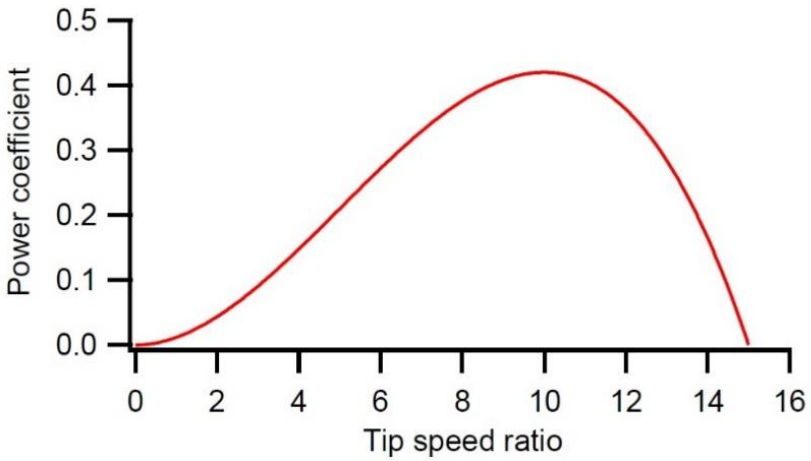

Figure 2 Power coefficient (Cp) Vs Tip speed ratio λ

power extraction however, in this research work system control is based on the variation of the load power requirement. Due to this control strategy, power extraction from turbine always tries to match the load requirement and hence, for certain load power scenarios the system tries to maximise the power extraction and at other times it runs only as a controlled power supply.

The torque at the turbine shaft produced by the wind is given by [12]

$$T_t = 0.5\pi\rho C_t r^3 v_w^2 \qquad (2.c)$$

where, $C_t = C_p/\lambda$ is the torque coefficient.

DC Generator

The armature of the DC generator is modelled as an RLE circuit, with E representing the back emf (electromotive force) in the armature when the rotor rotates due to the wind turbine. Denoting the generated voltage as V, the electrical and mechanical equations of the generator can be written as

$$\frac{di}{dt} = -\frac{R}{L}i + \frac{K_b}{L}\omega - \frac{1}{L}V \qquad (2.d)$$

$$\frac{d\omega}{dt} = -\frac{T_{em}}{J} - \frac{B}{J}\omega + \frac{1}{J}T_t \qquad (2.e)$$

where i is the armature current, K_b is back-emf constant, ω is the rotational speed of the generator, V is the generator voltage, J is the rotor inertia, B is the viscous-friction coefficient, T_t is the turbine torque and, T_{em} is the torque developed by the generator.

The developed electromagnetic torque T_{em} is given by

$$T_{em} = K_i * i \qquad (2.f)$$

where, K_i is the torque constant.

The voltage generated by the DC generator passes through power electronics interface to power the LED (light emitting diode) load bank. This power electronics interface (further discussed in chapter 5) consists of two DC-DC converters. The DC-DC buck converter is used to control the rotational speed of the generator shaft and the DC-DC boost converter is used to provide the required voltage to the load.

The DC-DC buck converter is based on a MOSFET (metal-oxide-semiconductor-field-effect transistor) connected in series with the armature of the generator. This MOSFET allows the flow of current to the load by switching its gate ON, which will produce electromagnetic torque T_{em} as expressed in Eq. (2.f). This torque will act against the turbine torque T_t to reduce the generator speed following the dynamic expressed in Eq. (2.e). In case of speed increase, the gate of the MOSFET is switched OFF and the generator operates under no load with only the turbine torque affecting its speed variation. When the speed reached the reference and to maintain it at that level, the gate keeps switching ON-OFF depending on the current error e_{ti} as follows

$$e_{ti} = i_T - i_{Tref} < 0 \ \rightarrow gate : ON \ \rightarrow \omega \downarrow \quad (2.g)$$

$$e_{ti} = i_T - i_{tref} > 0 \ \rightarrow gate : OFF \rightarrow \omega \uparrow \quad (2.h)$$

where, i_{tref} is the turbine current reference and i_T turbine current.

The switching ON-OFF of the gate is achieved by a PWM (pulse width modulated) signal generated from a controller for load power matching. The following section explains how this control is implemented in the physical system and how the power control is achieved using a DC-DC buck converter.

2.3. Wind Turbine Converter and Control

The basic circuit of a Buck converter is shown below in Figure 3. Two switches are used in this basic circuit, usually, one controlled (MOSFET) and one uncontrolled (diode), to achieve unidirectional power flow from the input to the output. This circuit, also, uses one

capacitor and one inductor to store and transfer energy from input to output. They, also, filter or smooth voltage and current.

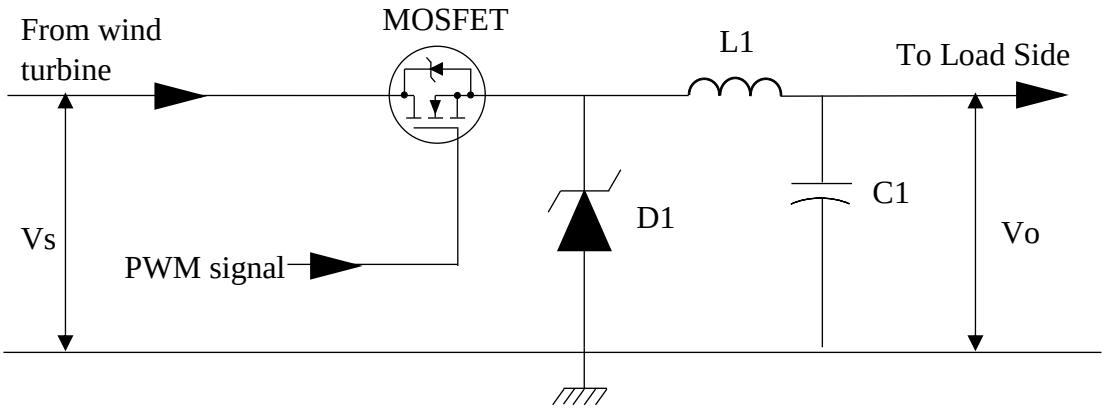

Figure 3 Turbine buck converter

In the above block diagram of the converter, Vs is Supply Voltage, D1 is Diode, C1 is Capacitor, L1 is an inductor and Vo is Output Voltage. The output voltage and current waveforms representation of the circuit (Fig. 3) are shown in Fig. 4.

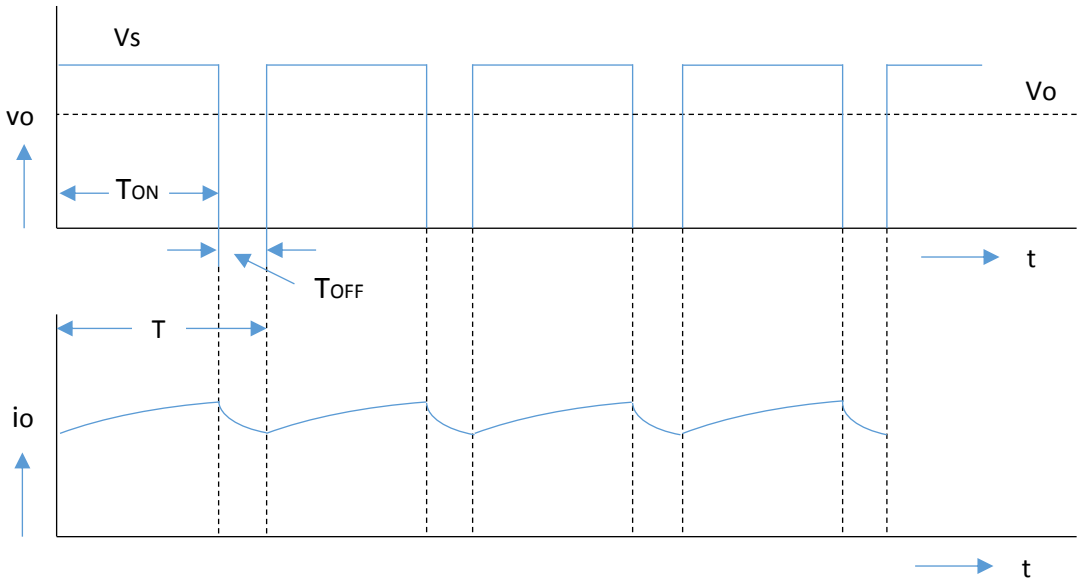

Figure 4 Buck converter output voltage and current waveform

The output voltage is same as the input voltage, i.e., $v_0 = V_s$, when the switch is ON, during the period, $T_{ON} \geq t \geq 0$. The switch is turned on at ON t = 0, and then turned off at $t = T_{ON}$. This is called ON period. During the next time interval, $T \geq t \geq T_{ON}$, the output voltage is zero, i.e., $v_0 = 0$, as the diode, D_F now conducts. The OFF period is $T_{OFF} = T - T_{ON}$, with the time period begin $T = T_{ON} + T_{OFF}$. The frequency is $f = 1/T$. With T kept constant, the average value of output voltage is,

$$V_0 = \frac{1}{T}\int_0^T v_0 dt = \frac{1}{T}\int_0^{T_{ON}} V_s dt = V_s\left(\frac{T_{ON}}{T}\right) = kV_s \qquad (2.i)$$

The duty ratio is $k = (T_{ON}/T) = [T_{ON}/(T_{ON} + T_{OFF})]$, its range being $1.0 \geq k \geq 0.0$. Normally, due to turn-on delay of the device used, the duty ratio (k) is not zero, but has some positive value. Similarly, due to requirement of the turn-off time of the device, the duty ratio (k) is less than 1.0. So, the range of duty ratio is reduced. The load current increases in the ON period, as the input voltage appears across the load, and it (load current) decreases in the OFF period, as it flows in the diode, but is positive at the end of the time period, T.

The control system of a wind energy conversion system is based on the equations (2.g) and (2.h) as explained in the previous section. In the wind turbine system, used in this work, a current control is carried out with the simple PI (proportional integral) based controller. Power management algorithm is used to provide the current reference to be tracked and, to maintain a proper functioning of the load, the voltage controller is integrated at the load side. The buck converter used for implementing the current control is as shown in the Fig. 3.

At the system start, the power management algorithm checks the potentially available power from the wind turbine based on the available wind speed. The algorithm further checks the load requirement and based on available power and loads requirement algorithm generates the current reference. This current reference is then used to generate the current error e_{ti}, as shown in the equation 2.h and 2.g. This error signal e_{ti} is sent to the PI controller, which generates a control signal in the form of duty cycle. To implement Proportional-Integral (PI) based current controller to track the current reference provided by the power management algorithm.

$$V^* = K_P e_{ti}(t) + K_I \int e_{ti}(t)dt \quad (2.j)$$

where, $e_{ti}(t) = i(t) - i^*(t)$ is the current error.

The output from the PI (proportional integral) controller i.e. duty cycle ($V^*/100 = k$) from equation (2.i), is converted to the PWM signal and sent to MOSFET on the power electronic interface using the digital output (discussed in Chapter 5).

Chapter 3 Solar Photovoltaic Energy System

3.1. Introduction

This chapter demonstrates the fundamental components and control strategy used in solar energy conversion system. Mathematical equations for the solar cell is briefly discussed along with solar PV characteristics IV (current-voltage) curve using open circuit voltage and short circuit current. This chapter also discusses the solar PV converter and its control in detail. This chapter also describes design and implementation of the current control loop, which is used to control DC-DC buck converter, to regulate the output current.

3.2. Solar Panel Modelling and Characteristics

Solar cells are the basic components of photovoltaic panels. Most are made from silicon even though other materials are also used. Solar cells take advantage of the photoelectric effect: the ability of some semiconductors to convert electromagnetic radiation directly into electrical current. The charged particles generated by the incident radiation are separated conveniently to create an electrical current by an appropriate design of the structure of the solar cell.

Fig. 5 shows the Solar PV panel used in this Hybrid Energy system. This PV panel contains 60 solar cells connected in series. The solar cell can be represented by the electrical model shown in Fig. 6. Its current-voltage characteristic is expressed by the following equation [20]

$$I = I_L - I_0\left(e^{\frac{q(V+IR_S)}{AkT}} - 1\right) - \frac{(V+IR_S)}{R_{SH}} \quad (3.a)$$

where I and V are the solar cell output current and voltage respectively, I_L is the light generated current, I_0 is the dark saturation current, q is the charge of an electron, A is the diode quality (ideality) factor, k is the Boltzmann constant, T is the absolute temperature and R_S and R_{SH} are the series and shunt resistances of the solar cell. R_S is the resistance offered by the contacts and the bulk semiconductor material of the solar cell. The origin of the shunt resistance R_{SH} is more difficult to explain. It is related to the non-ideal nature of the p–n junction and the presence of impurities near the edges of the cell that provide a short-circuit path around the junction. In an ideal case R_S would be zero and R_{SH} infinite. However, this ideal scenario is not possible, and manufacturers try to minimize the effect of both resistances to improve their products.

Figure 5 Solar PV panel

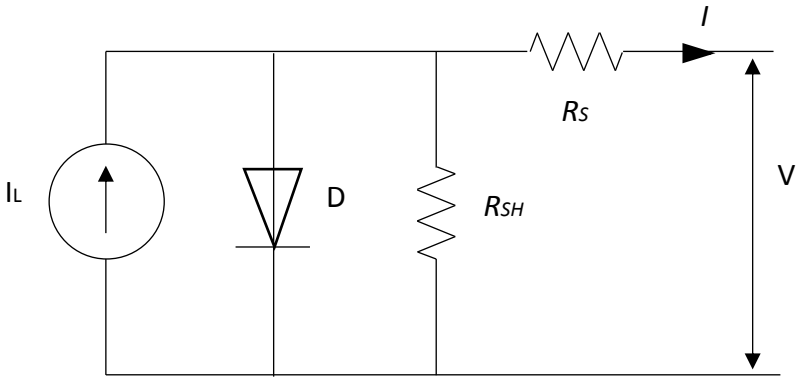

Figure 6 Equivalent circuit of the solar cell

Sometimes, to simplify the model, the effect of the shunt resistance is not considered, i.e. R_{SH} is infinite, so the last term in (3.a) is neglected. A PV panel is composed of many solar cells, which are connected in series and parallel so the output current and voltage of the PV panel are high enough to the requirements of the grid or equipment. Considering the simplification mentioned above, the output current-voltage characteristic of a PV panel is expressed by equation (3.b), where n_P and n_S are the number of solar cells in parallel and series respectively. [20]

$$I \approx n_P I_L - n_P I_0 \left(e^{\frac{q(V+IR_S)}{AkTn_S}} - 1 \right) \quad (3.b)$$

Open Circuit Voltage, Short Circuit Current and Maximum Power Point:

Two important points of the current-voltage characteristic are: the open circuit voltage V_{OC} and the short circuit current I_{SC}. At both points, the power generated is zero. V_{OC} can be approximated from (3.a) when the output current of the cell is zero, i.e. I = 0 and the shunt resistance R_{SH} is neglected. It is represented by equation (3.c). The short circuit current I_{SC} is the current at V = 0 and is approximately equal to the light generated current I_L as shown in equation (3.d). [21]

$$V_{OC} \approx \frac{AkT}{q} \ln\left(\frac{I_L}{I_0} + 1\right) \quad (3.c)$$

$$I_{SC} \approx I_L \quad (3.d)$$

The maximum power is generated by the solar cell at a point of the current-voltage characteristic where the product $V_M I_M$ is maximum. This point is known as the MPP and is unique, as can be seen in Fig. 7 [21], where the previous points are represented.

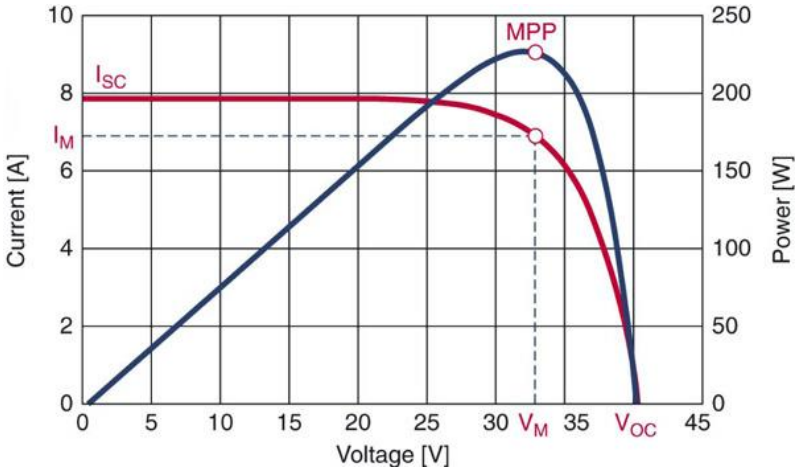

Figure 7 Solar cell characteristic IV curve

3.3. Solar PV Converter and Control

The basic circuit of a buck converter used in this system is as shown below in Figure 8. Two switches are used in this basic circuit, usually, one controlled (MOSFET) and one uncontrolled (diode), to achieve unidirectional power flow from the input to the output. This circuit, also, uses one capacitor and one inductor to store and transfer energy from input to output. They, also, filter or smooth voltage and current.

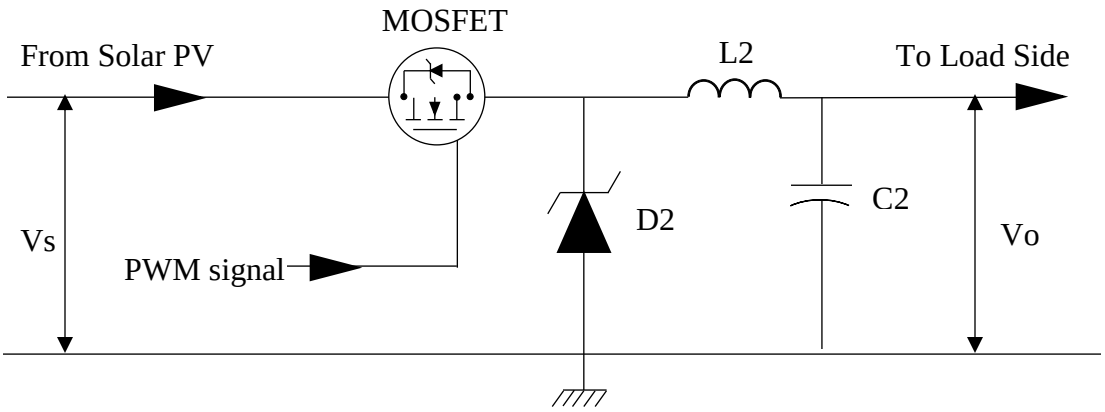

Figure 8 Solar PV buck converter

In the above block diagram of the converter, Vs is Supply Voltage, D2 is Diode, C2 is Capacitor, L2 is an inductor and Vo is Output Voltage.

The output voltage and current waveforms representation of the circuit (Fig. 8) are shown in Fig. 9.

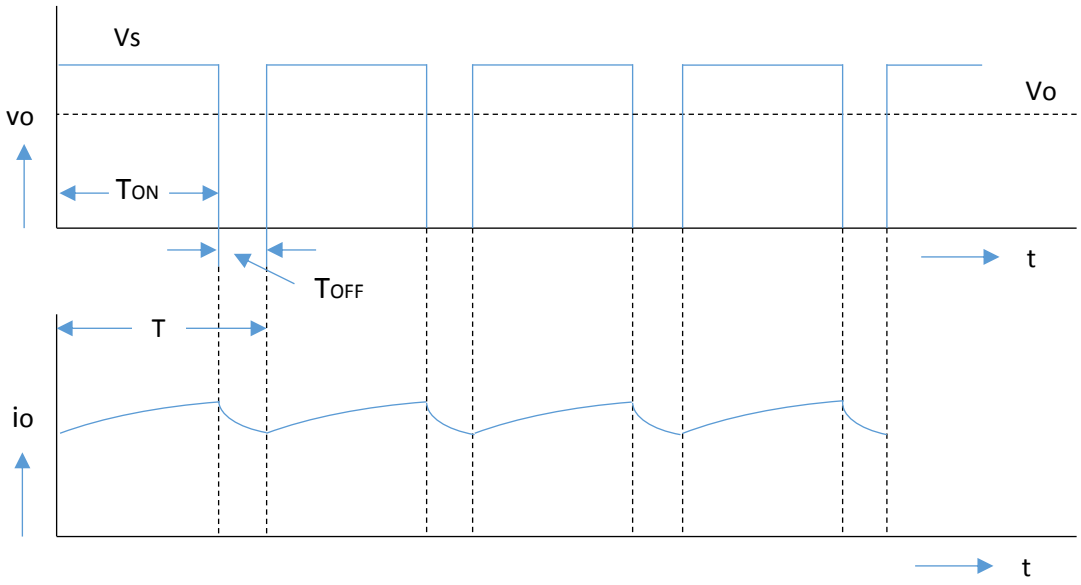

Figure 9 Buck output voltage and current waveform

The output voltage is same as the input voltage, i.e., $v_0 = V_s$, when the switch is ON, during the period, $T_{ON} \geq t \geq 0$. The switch is turned on at ON t = 0, and then turned off at $t = T_{ON}$. This is called ON period. During the next time interval, $T \geq t \geq T_{ON}$, the output voltage is zero, i.e., $v_0 = 0$, as the diode, D_F now conducts. The OFF period is $T_{OFF} = T - T_{ON}$, with the time period begin $T = T_{ON} + T_{OFF}$. The frequency is $f = 1/T$. With T kept constant, the average value of output voltage is,

$$V_0 = \frac{1}{T}\int_0^T v_0 dt = \frac{1}{T}\int_0^{T_{ON}} V_s dt = V_s\left(\frac{T_{ON}}{T}\right) = kV_s \qquad (3.e)$$

The duty ratio is $k = (T_{ON}/T) = [T_{ON}/(T_{ON} + T_{OFF})]$, its range being $1.0 \geq k \geq 0.0$. Normally, due to turn-on delay of the device used, the duty ratio (k) is not zero, but has some positive value. Similarly, due to the requirement of the turn-off time of the device, the duty ratio (k) is less than 1.0. So, the range of duty ratio is reduced. The load current increases in the ON period, as the input voltage appears across the load, and it (load current) decreases in the OFF period, as it flows in the diode, but is positive at the end of the time-period, T.

The control system for solar PV energy system is based simple current loop as explained in the previous section. In the solar PV system, used in this work, a current control is carried out with the simple PI (proportional integral) based controller. Power management algorithm is used to provide the current reference to be tracked and, to maintain a fixed voltage at the load side, the voltage controller is integrated, which provides the fixed voltage. The buck converter used for implementing the current control is as shown in the Fig. 8.

At the system start, the power management algorithm checks the power from the solar PV. The algorithm further checks the load requirement and based on available power and loads requirement algorithm generates the current reference. This current reference is then used to generate the current error e_{pi}, as shown below. This error signal e_{pi} is sent to the PI controller, which generates control signal in the form of duty cycle. To implement Proportional-Integral (PI) based current controller to track the current reference generated by the power management algorithm.

$$U^* = K_P e_{pi}(t) + K_I \int e_{pi}(t)dt \quad (3.f)$$

where, $e_{pi}(t) = i(t) - i^*(t)$ is the current error.

The output from the PI controller i.e. duty cycle ($U^*/100 = k$) from equation (3.e), is converted to the PWM signal and sent to MOSFET present on the power electronic interface using the digital output (discussed in Chapter 5).

Chapter 4 Power Management System Algorithm

Introduction

As the number of energy sources is increased in the system complexity to control and maintain the power balance becomes a critical challenge in the hybrid energy systems or in DG (Distributed generation) systems. This chapter briefly discusses the power management system(PMS) and why it is needed in today's scenario. Further, a brief introduction is given to the hybrid energy system, which is designed and used in this work. Also, PMS algorithm designed for this work is introduced and discussed. Lastly, various power requirement conditions are introduced and PMS algorithm approach in each condition is looked at.

4.1 Power Management System

One of the main problems of the HES (hybrid energy system) or DG is related to the control and supervision of the energy distribution. The dynamic interaction between the grid and/or the loads and the power electronic interface of the renewable source can lead to, critical problems of stability and power quality in the new system, that are not very common in conventional power systems. Managing the flow of power throughout the proposed system to assure a continuous supply of the load demand is achieved. The main objective of the power flow and management system is to supply the load with its full demand. One possible approach emerged in this kind of challenge is to have a centralized power monitoring from all possible sources of power supply and power demand. With the

centralized monitoring, data needed to balance the supply and demand is available to be employed in the decision making to effectively control the power flow. Decision making can then be designed based on various factors such as sources of generation, cost of power, priority loads, weather forecasting etc. As the DGs are increasing and getting connected to the grid, this evolving smart grid of multiple microgrids makes it imperative to have PMS based on various factors introduced before.

In this research, project power is generated from the Wind turbine and Solar PV. Power coming from both the energy sources is controlled by the control loop using buck converters interfaced with energy sources on the power electronics interface. The power which is controlled using individual buck converters is combined at the DC link before boost converter and then fed to the LED load bank. Since the system has two power sources it becomes imperative to manage the power between the two to control the overall system reliably.

Next section discusses the developed PMS algorithm in detail however certain conditions were considered before designing the condition loops to control the power flow.

Power supply form the Solar PV is higher than the wind turbine system hence, the cost function is designed to take more power from the solar PV than the wind turbine by the ratio of 3:2.

If the user overrides the algorithm and gives the user input load priority, then the system tries to match the load requirement. And if the power supply is not adequate then the user gets a warning prompt to adjust the load priority.

4.2 Hybrid Energy System Configuration

The hybrid energy system used for this work has wind energy system and Solar PV system as the power generation sources as discussed in chapter 2 and chapter 3 respectively. The load side configuration is discussed in detail in chapter 6. Here, detail configuration of the system is discussed along with control system implementation and signal communication between field parameters and control signals. This section also discusses power flow between sources and the load.

Fig. 10 shows the detailed configuration of the hybrid energy system. The schematic shows the signal flow to and from the controller modules and the power flow from the power generation to the load. Power flows from the Solar PV and DC generator to the DC-DC buck controller and to the DC-DC boost converter subsequently. From boost controller, the power is fed to the load through the switch which controls power to the load bank based on user priority or the PMS algorithm.

The voltage is measured at various points in the system to monitor power flow. The voltage measured by the voltage sensor on the power electronics interface is acquired through the analog voltage input module NI (National Instruments)-9201 (discussed in the section 5.2.2). The acquired voltage signals are used in the PMS algorithm to generate a current reference. The control system module inside the designed system uses the current reference value and real-time value to generate the control signal using the PI controller. The generated control signal, which is a PWM waveform, is implemented in the field using the digital output module NI-9401 (discussed in the section 5.2.3) and DC-DC converters. Q1-

cRIO module acquires the encoder signal from the field encoders to monitor the turbine speed and the blower speed.

The controller NI cRIO 9024 and the chassis NI-9112 holds the data acquisition modules mentioned before and runs the real-time system. cRIO controller communicates the data to and from the desktop computer using Ethernet communication protocol. The desktop computer has the interface which takes user input and displays various system parameters to monitor the system.

The load is controlled using the digital ON/OFF signal generated by PMS algorithm and implemented using the digital output from NI-9401 module and MOSFET as a switch on the power electronics interface.

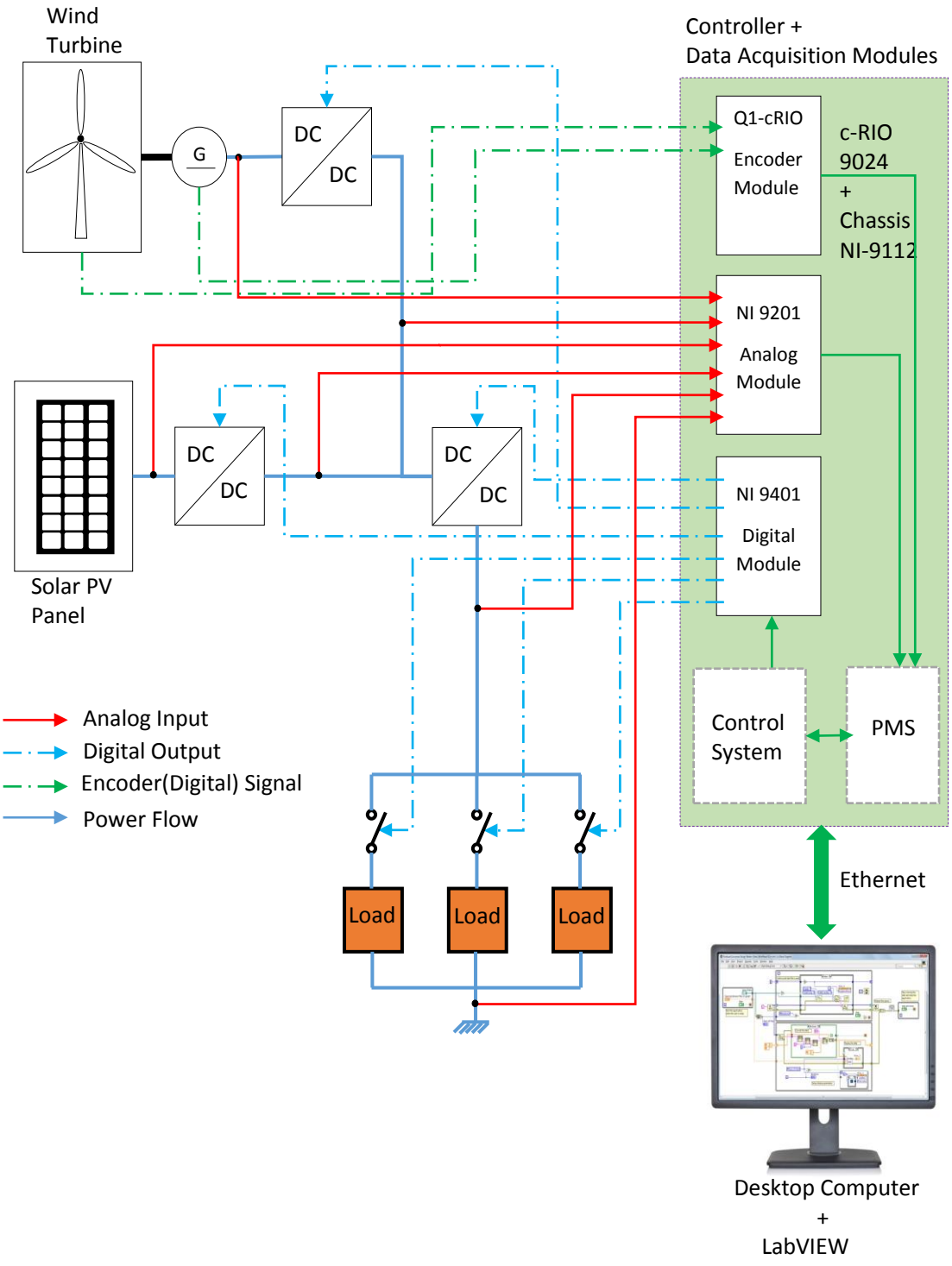

Figure 10 Hybrid energy system configuration

4.3 Power Management System Algorithm

PMS algorithm is mainly based on five field measurement variables which are required to run the system reliably. These are 1) Wind Speed (W_s) 2) Solar PV current (i_{PV}) 3) Wind turbine current (i_T) 4) Load current (i_L) 5) Solar PV voltage (V_{PV})

4.3.1 PMS Algorithm (Auto mode)

The flow charts in the fig. 11 and fig. 12 are the representation of the PMS algorithm designed for this research project. The algorithm starts with the measurement of the field parameters mentioned before, this process is represented by the parallelogram block, which represents system input and output. The measured field parameters are used in the following function.

$$F(W_s, i_{PV}) = \begin{cases} W_{co} < W_s \leq W_h, i_{PV} < i_{PV1} \\ W_s \geq W_h, i_{PV1} < i_{PV} < i_{PV2} \\ W_s \geq W_h, i_{PV} \geq i_{PV2} \end{cases} \quad (5.a)$$

Where, W_{co} is wind cut-off speed, W_h is high wind speed, i_{PV1} & i_{PV2} are the solar PV current references, which are based on the load. Also, here $i_{PV1} < i_{PV2}$.

Results from the equation 5.a are used further to decide the priority load and the reference load current. This process is carried out in the subsequent stage, where results from the function in 5.a lead to unique three cases. These three cases are used as follows to decide the load current reference and load switches to be kept ON.

Case 1.

$$F(W_s, i_{PV}) = W_s \geq W_h, i_{PV} \geq i_{PV2} \rightarrow L_1 \& L_2 \& L_3 \quad (5.b)$$

In this case, both the power generation sources generate maximum or adequate power to keep all the loads ON hence, all three i.e. L_1, L_2 and L_3 are kept ON and the load current

reference is kept at 90 mA, this value is based on the system components and design specifications of the power electronics interface circuit.

Case 2.

$$F(W_s, i_{PV}) = W_s \geq W_h, i_{PV1} < i_{PV} < i_{PV2} \rightarrow L_1 \& L_2 \quad (5.c)$$

In this case, medium power output from the solar PV and DC generator allow two load banks to be switched ON hence, L_1 and L_2 are given priority and load current reference it kept at 60 mA.

Case 3.

$$F(W_s, i_{PV}) = W_{co} < W_s \leq W_h, i_{PV} < i_{PV1} \rightarrow L_1 \quad (5.d)$$

In this case, since power is low only one load is switched ON (L_1 in this algorithm) and load current reference is kept at 30 mA.

The load current reference generated in the above process is used to generate references for individual power supply sources since each source is controlled using separate DC-DC buck converters. i.e. solar PV buck converter and wind turbine buck converter are controlled independently but the total current at the load side is a combination of the current coming from both the sources.

In this system solar PV has higher power generation capacity than the wind turbine system hence, solar PV contributes more power to the load. This fact is utilized in the current reference generation for the individual sources specifically in the case 1 mentioned above. In case 1, reference load current is divided in the ration 3:2, and higher value is assigned to solar PV current reference and the lower of the two is assigned to the wind turbine current reference. This process is carried out using following equation.

$$i_{PVref} = 0.6 * \ i_{Lref} \quad (5.e)$$

$$i_{Tref} = 0.4 * \ i_{Lref}$$

Where, i_{PVref} is solar PV current reference, i_{Tref} is wind turbine current reference and i_{Lref} is load current reference.

In case 2, power supply from both the sources is similar hence, reference generation follows the equation 5.f

$$i_{PVref} = 0.5 * \ i_{Lref} \quad (5.f)$$

$$i_{Tref} = 0.5 * \ i_{Lref}$$

Where, i_{PVref} is solar PV current reference, i_{Tref} is wind turbine current reference and i_{Lref} is load current reference.

In case 3, both the power generation sources cannot match the load individually hence both solar PV current reference and wind turbine current reference is generated using equation 5.g

$$i_{PVref} = 1.0 * \ i_{Lref} \quad (5.g)$$

$$i_{Tref} = 1.0 * \ i_{Lref}$$

Where, i_{PVref} is solar PV current reference, i_{Tref} is wind turbine current reference and i_{Lref} is load current reference.

Based on the references generated in the above process error signal i.e. $\delta i_{PV}, \delta i_T$ is generated using the equation 5.h

$$\delta i_{PV} = i_{PV} - i_{PVref} \quad (5.h)$$

$$\delta i_T = i_T - i_{Tref}$$

Where, i_{PVref} is solar PV current reference, i_{Tref} is wind turbine current reference, i_{PV} is instantaneous solar PV current and i_T is instantaneous wind turbine current.

The error signal from the equation 5.h is used to generate the control signal using a PI controller (discussed in chapter 2 and 3). This control signal either increases or decreases the duty cycle of the buck converter depending on the sign of the error signal being positive or negative, i.e. if the error signal is positive then the instantaneous value of i_{PV} or i_T is greater than the reference duty cycle of the buck converter signal is reduced to lower the current output and vice versa. This process is executed in the subsequent step after the error signal generation. Final process in this algorithm is to verify whether the new instantaneous current from both sources meets the load demand and its done using equation 5.i given below.

$$i_L = i_{PV} + i_T \tag{5.i}$$

If the equation 5.i is satisfied, then the algorithm goes back to the monitoring function $F(W_s, i_{PV})$ and if the equation 5.i is not satisfied by the system current outputs then the algorithm goes back to the reference generation stage as shown in the algorithm flow chart in the fig 11.

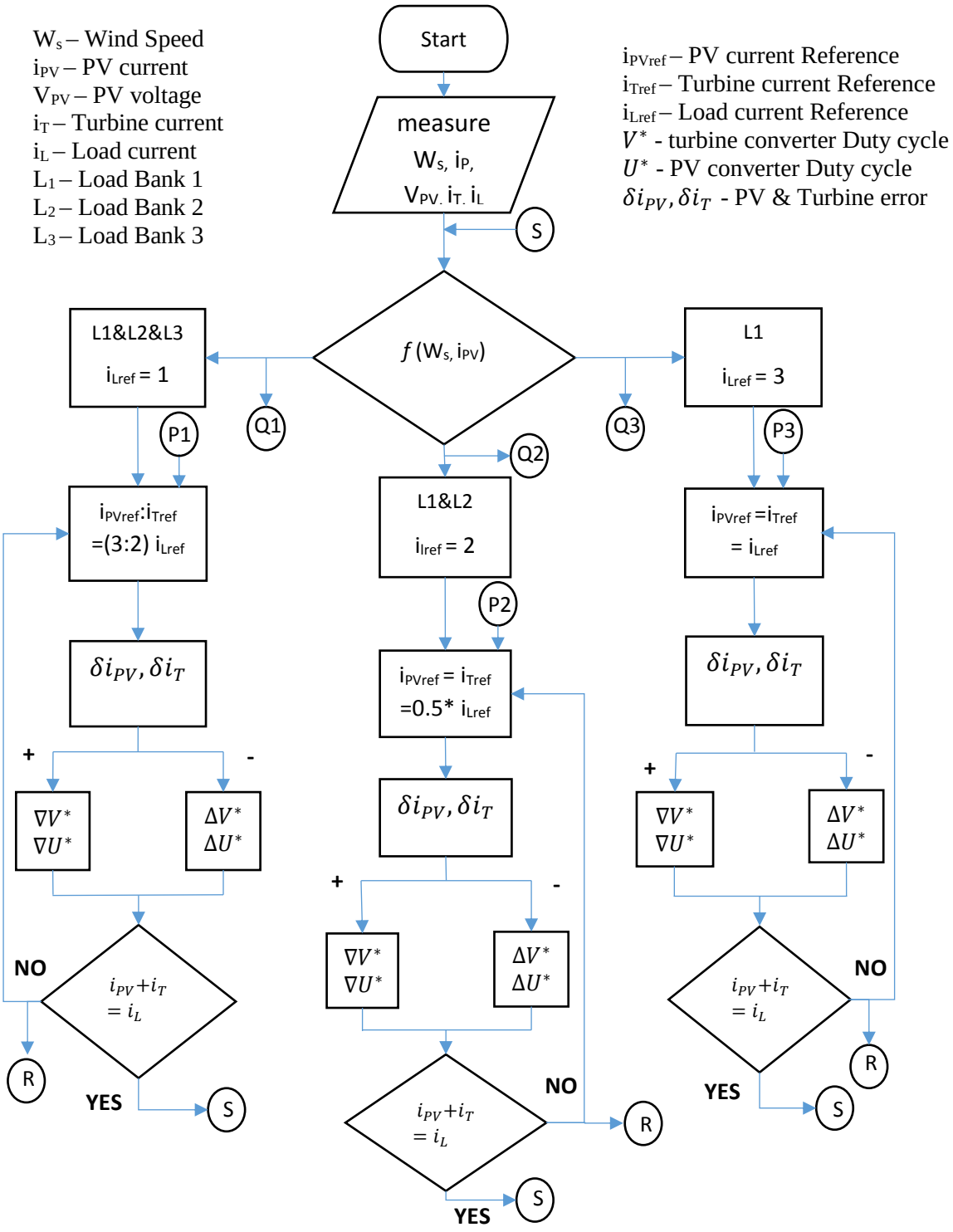

Figure 11 PMS algorithm (Auto mode)

4.3.2 PMS Algorithm (Manual mode)

In this mode of operation, PMS algorithm performs a similar function as in the auto mode discussed in the previous section except for the autoload switching i.e. in this mode user has the control to decide the priority from the front panel interface of the system. Fig 12 shows the flowchart of the PMS algorithm in manual mode. This manual mode of PMS algorithm uses the parts of the auto mode from the previous section in certain sections of the decision making for load current reference generation.

The PMS algorithm is switched into manual mode is using auto mode switch on the front panel interface of the system (discussed in section 5.3). In this mode user input is expected for the load priority. After the user input is taken, algorithm check the monitoring function $F(W_s, i_{PV})$ for available power generation capacity. Based on the cases discussed in previous section algorithm returns the value, this is represented by the Q1, Q2 and Q3 in the flow chart. The returned value is than compared to the user input load demand i.e. user input decides the load current reference which is then compared to the value returned from the monitoring function. If the power supply is equal or greater than the load demand, then the system tries to meet the load demand. But, if the load demand is higher than the supply potential the system tries to match the demand by increasing the duty cycle and waits for 10 seconds. At the end of the 10 second countdown timer algorithm prompts the user to reduce the load as the system cannot provide enough power to power all the loads user wants. If during the countdown time the system provides supplies the required power, then the timer is reset and waits for the next trigger point (low power situation).

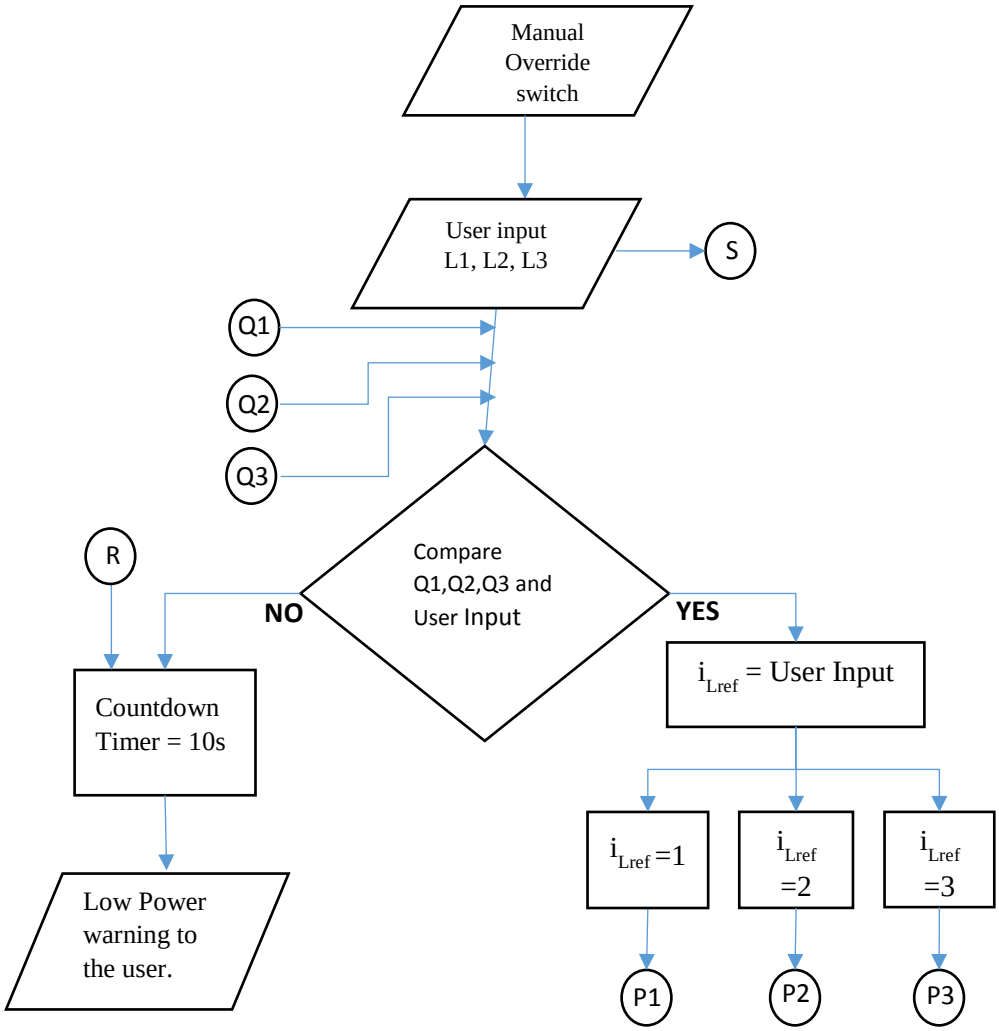

Figure 12 PMS algorithm (Manual mode)

Chapter 5 NI-LabVIEW Based Control Interface

5.1. Introduction

This chapter gives a brief introduction to the important system components used in this research work and their role in rapid control prototyping is looked at from this research project perspective. Apart from the hardware system components, another major component is the software control interface. In the following sections, the control interface is discussed in detail.

This hybrid energy system consists of power electronics interface, three different data acquisition modules to acquire data from the filed and send a control signal to the field, a controller with the chassis to hold the data acquisition modules. The following section expands on each of these components.

5.2 Rapid Control Prototyping Components

As shown in fig 10 in chapter 4, a desktop computer is used as the development computer, NI cRIO 9024 with chassis and modules are the Real-time target machine acting as controller and power electronics interface consisting of DC-DC converters is hardware in the loop. All these system components are used together for rapid control prototyping with minimum role over time for the different control designs. These real-time targets allow the control design to be rapidly run, monitored and tested.

5.2.1. NI cRIO 9024

This model of cRIO features an industrial 800 MHz real-time processor for deterministic, reliable real-time applications and contains 512 MB of DDR2 RAM and 4 GB of non-volatile storage for holding programs and logging data. The controller communicates with the desktop using Ethernet port to conduct programmatic communication over the network and built-in web (HTTP) and file (FTP) servers. The developed LabVIEW software interface can run on cRIO or desktop. Also, cRIO is used to facilitate the communication between desktop and FPGA hardware for real-time monitoring and performance analysis of the control system algorithms. [51]

Figure 13 NI cRIO-9024

5.2.2. Q1-cRIO module

This module contains two encoder inputs, an analog input (±10V) and an analog output (±10V) terminal. The Analog output terminal is used to send speed control signal to the blower fan. This analog output signal is sent to a linear voltage-controlled power amplifier (VoltPAQ-X1 Power Module), which amplifies the signal to run the blower. Blower fan speed information is obtained using feedback from an encoder sensor through an encoder input terminal on the module. Fig. 16 shows the Q1-cRIO module and it's I/O terminals. [52]

Figure 14 Q1-cRIO module

5.2.3. NI 9201 Analog Input module

This module contains 8 Analog Inputs (±10 V) with sample rate 500kS/s and 12-bit resolution [53]. Analog inputs in this module are used to acquire voltage sensor data from power electronics interface. As shown in the general schematic of power electronics interface in Fig 21, a total of 8 voltage sensors present in this system and this module has required inputs terminals to serve the purpose. Fig 17 shows the NI 9401 Analog input module.

Figure 15 NI 9201 Analog input module

5.2.4 NI 9401 Digital I/O module

This module contains 5 V/TTL, Bidirectional Digital I/O, 8 channels. Three outputs are used to send control algorithm generated PWM signal to each DC-DC converters and remaining outputs are used as the digital switches to control LED load banks. Fig 18 shows the NI 9401 Digital I/O module

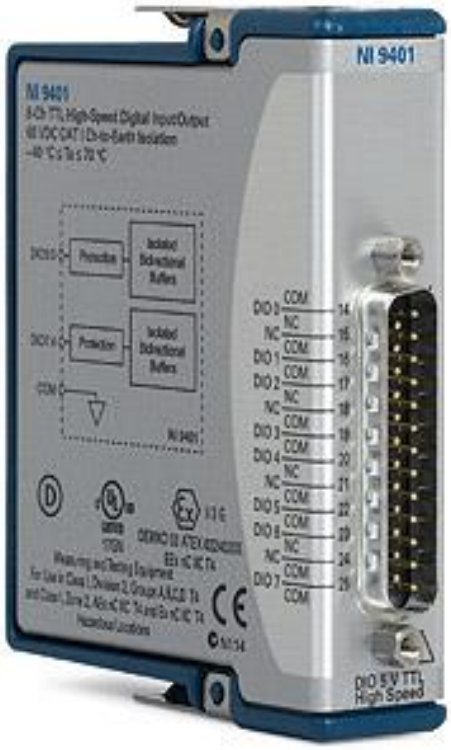

Figure 16 NI 9401 Digital output module

5.3. LabVIEW Control Interface

The LabVIEW control interface designed for this system is divided into two parts 1) User level interface and 2) Operator level interface.

1) User level Interface

This control interface is designed for the user or a non-technical user, the front panel of this interface is shown in fig 19. This user interface gives options to the user to use the system in auto or in manual mode and takes the user input for the required load when in manual mode. The user interface has the representation of the load bank present on the power electronics interface, this shows the real-time state of the load bank by changing the colour to black (for OFF state) or red (for ON state).

The user interface has the power generation representation as a pie chart as well as the value is presented in the wattmeter section. The pie chart shows the share of power generated from both the sources, i.e. solar PV and wind turbine generator, to supply the load demand.

2) Operator level Interface

This control interface has options to tune the PI controller parameters. The operator level interface has various important system parameters to observe the system response in detail. These parameters include turbine and blower speed and power, voltage and current outputs of the total energy system. Fig 20 shows the operator control interface

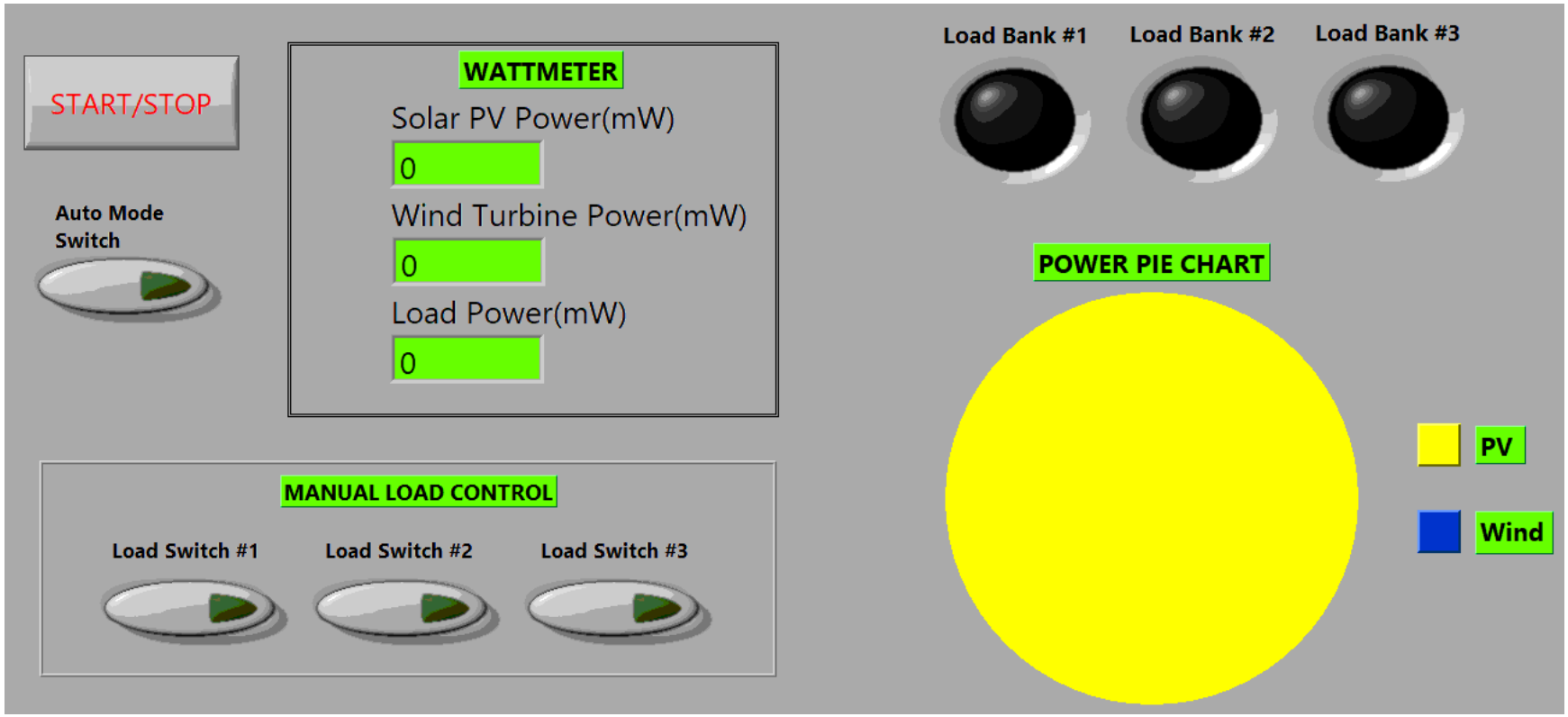

Figure 17 Front panel (user control interface)

Figure 18 Front panel (operator control interface)

5.4 Instrumentation and Measurement

Important hardware component in this system is the power electronics interface, a general schematic of which is represented in fig 21. Power electronics board is used for implementing the DC-DC converter configuration designed for the energy system in this research work. This board also contains the measurement sensors with instrumentation amplifiers for sending field measurements to the data acquisition modules described in the previous section. Fig 21 gives the detail representation of the sensor connections and signal flow in this system.

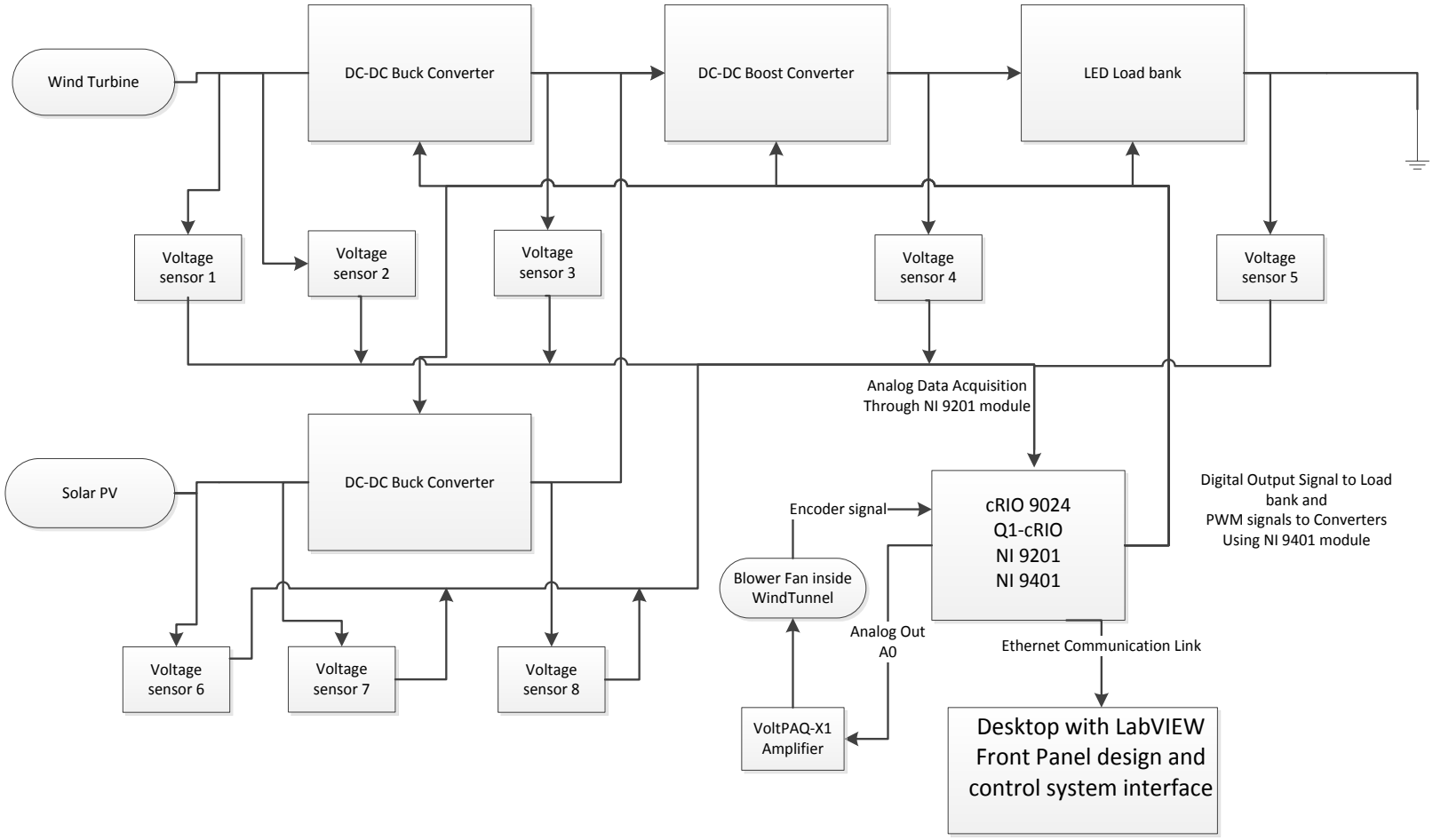

Figure 19 General schematic of the system

Chapter 6 Experimentation and Results

6.1 Introduction

This chapter gives a brief account of the experimental system setup and the hardware components in the initial sections. The following section introduces the load side configuration which includes DC-DC boost converter and load bank. The final section gives detailed experimental results and discussion about the same for various experimental cases.

6.2 Experimental Setup

The system used for this experiment consists of the wind turbine generator system (chapter 2), solar PV energy system (chapter 3) as energy sources connected to DC-DC buck converters respectively as current loop controllers. From both the DC-DC buck converters system is connected to single DC-DC boost converter which is used as the voltage regulator at the load side (further discussed in section 6.3). After the DC-DC boost converter load bank is connected to the switch to control the load bank.

6.3 Load Side Configuration

The energy generated from both the sources (wind turbine and solar PV) is used to power the LED load bank. The Load bank is designed using LED's arranged in six rows, each containing 2 LEDs in series with a resistance. Every row had MOSFET as a switch to control the load bank digitally through a software interface. The uncontrolled DC-DC boost converter ensures the voltage supply needed for the load bank, however, the brightness of

the lights depends on the incoming current supply to the load. Fig 20 shows the basic schematic of the load bank used in this system.

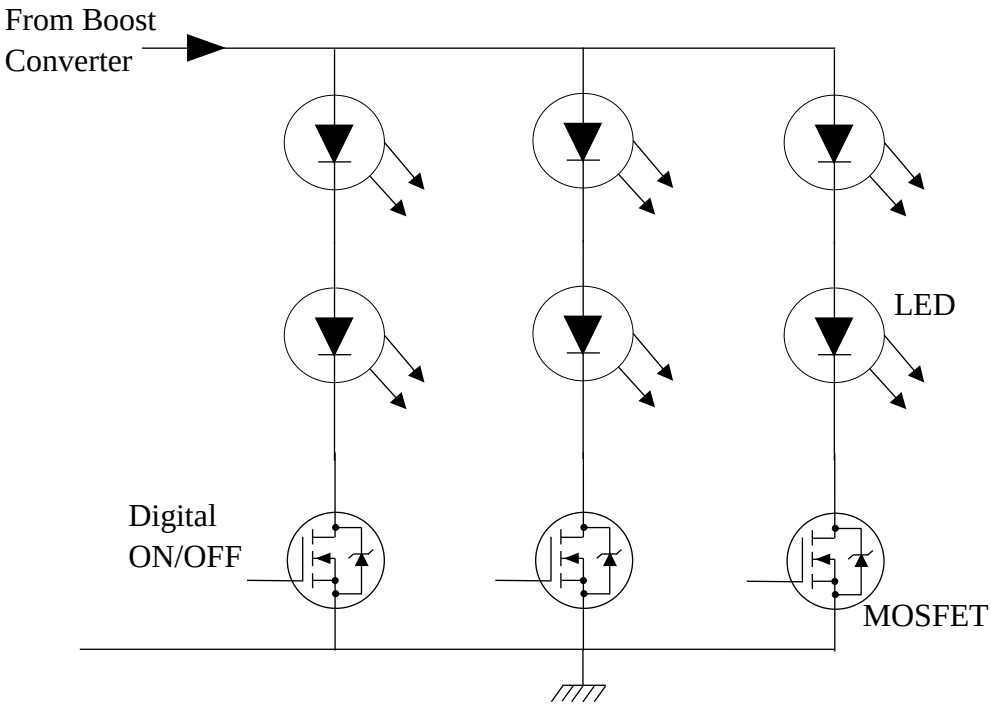

Figure 20 Load bank

The load side converter control system is used to regulate the voltage V_L across the load to maintain a proper functioning of the LED based load. The voltage controller is based on a PI regulator with gains Kp and Ki

$$J^* = K_p(V_L - V_L^*) + K_i \int (V_L - V_L^*)dt \quad (6.a)$$

Its output is the firing signal to be delivered to the gate of the MOSFET in the DC-DC boost converter. The basic circuit of a Boost converter is shown in Figure 22

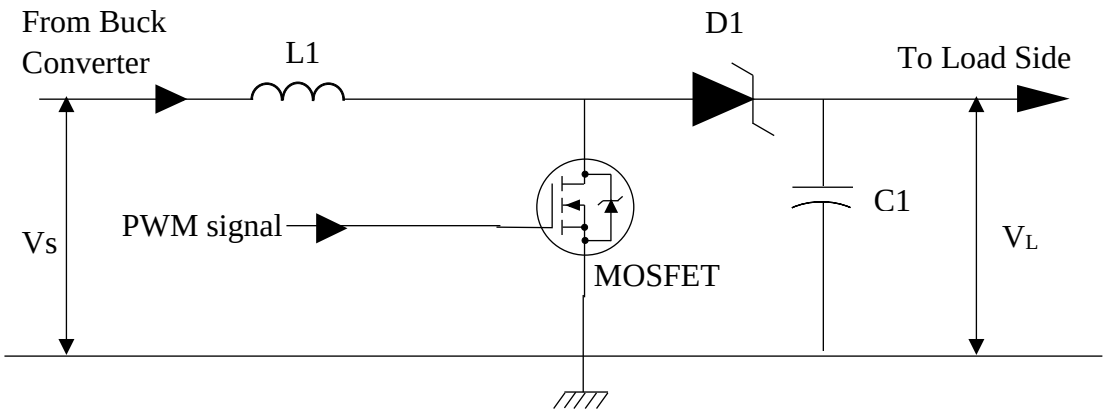

Figure 21 DC-DC boost converter

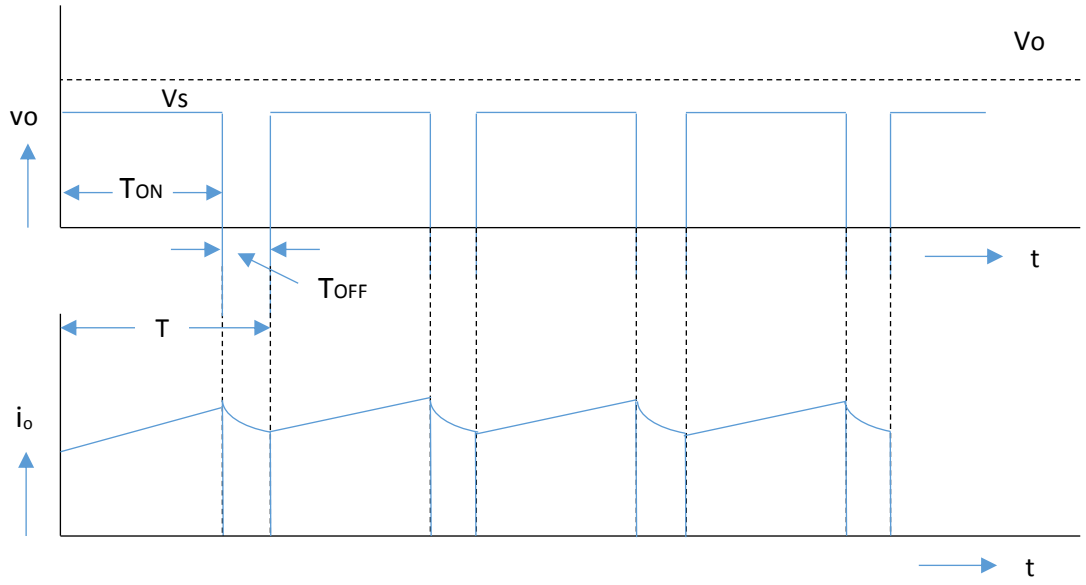

Figure 22 Boost converter voltage and current waveform

Firstly, the switch, S (i.e., the device) is put ON (or turned ON) during the period, $T_{ON} \geq t \geq 0$, the ON period being T_{ON}. The output voltage is zero ($v_0 = 0$). The current from the source (i_s) flows in the inductance L. The value of current increases linearly with time in this interval, with (di/dt) being positive. As the current through L increases the polarity of the induced emf is taken as positive, the equation of the circuit is,

$$V_s = L\frac{di_s}{dt} \quad or, \quad \frac{di_s}{dt} = \frac{V_s}{L} \tag{6.b}$$

The switch, S is put OFF during the period, $T \geq t \geq T_{ON}$, the OFF period being $T_{OFF} = T - T_{ON}$, with the time period begin $T = T_{ON} + T_{OFF}$. As the current through L decreases, with its direction being in the same direction as shown (same as in the earlier case), the induced emf reverses. So, the induced emf (taken as –ve in the equation given later) is added with the supply voltage, being of the same polarity, thus, keeping the current ($i_s = i_0$) in the same direction. The current ($i_s = i_0$) decreases linearly in the time interval, T_{OFF}, as the output voltage is assumed to be nearly constant at $v_0 \approx V_0$, with (di_s/dt) being negative, as $V_s < V_0$. The equation for the circuit is,

$$V_s = V_0 + L\frac{di_s}{dt} \quad or, \quad \frac{di_s}{dt} = \frac{(V_s - V_0)}{L} \tag{6.c}$$

The source current waveform is shown in Fig. 23. As stated earlier, the current varies linearly from I_1 (I_{min}) to I_2 (I_{max}) during the time interval, T_{ON}.

So, using the expression for di_s/dt during this time interval,

$$I_2 - I_1 = I_{max} - I_{min} = (V_s/L)T_{ON}. \tag{6.d}$$

Similarly, the current varies linearly from I_2 (I_{max}) to I_1 (I_{min}) during the time interval, T_{OFF}.

So, using the expression for di_s/dt during this time interval,

$$I_2 - I_1 = I_{max} - I_{min} = [(V_0 - V_s/L)]T_{OFF}. \tag{6.e}$$

Equating two equations (6.d) and (6.e), the average value of output voltage is,

$$V_0 = V_s\left(\frac{T}{T_{OFF}}\right) = V_s\left(\frac{T}{T - T_{ON}}\right) = V_s\left(\frac{1}{1-(T_{ON}/T)}\right) = V_s\left(\frac{1}{1-k}\right) \tag{6.f}$$

The time period is $T = T_{ON} + T_{OFF}$, and the duty ratio is $k = (T_{ON}/T) = [T_{ON}/(T_{ON} + T_{OFF})]$, its range being $1.0 \geq k \geq 0.0$. In this case, the output voltage is higher than the input voltage, as contrasted with the previous case of buck converter (dc-dc).

6.6 Results and Discussion

The power management system designed here can handle various scenarios with the uncertain weather, based on this assumption following 4 different experiment cases are tested to check the system response to the change. Four experiment test cases are as follows 1) Variable irradiance and constant wind speed and auto load adjustment. 2) Constant irradiance and variable wind speed and auto load adjustment. 3) Variable irradiance and wind speed and auto load adjustment and 4) Variable wind and irradiance and manual load adjustment. The following section gives details of the each of these test cases with the results.

Results attached in the following section are divided into to the structure as follows,

a) Discussion about the result
b) Power chart showing power response of solar PV and wind turbine generated power and load power consumption.
c) Voltage chart showing voltage at the power generation source and the load side
d) Current chart showing current at the power generation source and the load side

1) Experiment case 1: Variable irradiance and constant wind speed and auto load adjustment.

Fig 32 and 33 show the before and after scenario in the experiment case 1, as the algorithm is running in auto mode it can be observed that the load bank no.3 is switched off when the power from the solar PV is reduced due to low irradiance. It can also be observed that the in fig 33 share of wind power increases and is nearly equal to the power generated by the solar PV, this is due to the PMS algorithm forcing equal power extraction from both the sources in case of equal power generation by both the sources.

From fig 23 the spike in wind power generation occurs between time 00:25 to 00:30, this is due to current spike which occurs when lower irradiance causes current output from the solar PV to reduce (fig. 26) and in response current from wind turbine tries to compensate that before the PMS algorithm reduces the load.

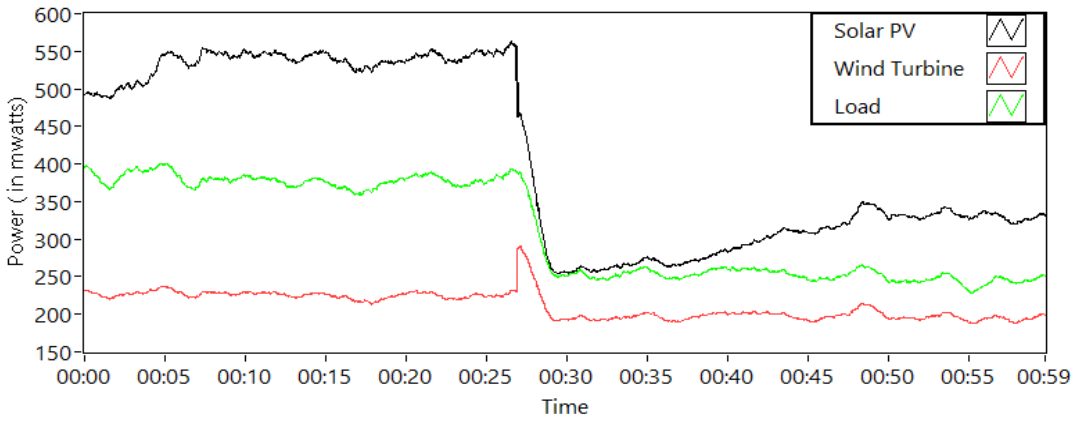

Figure 23 Experiment case 1: power response

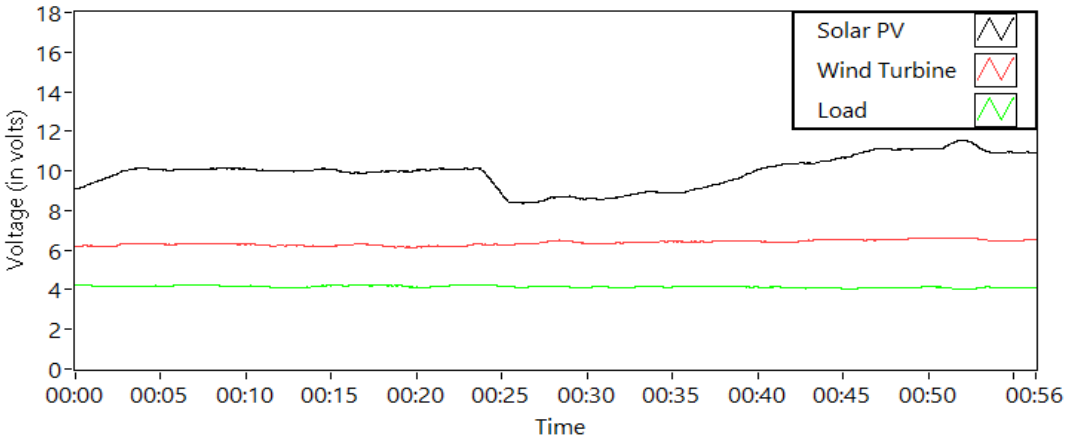

Figure 24 Experiment case 1: voltage response

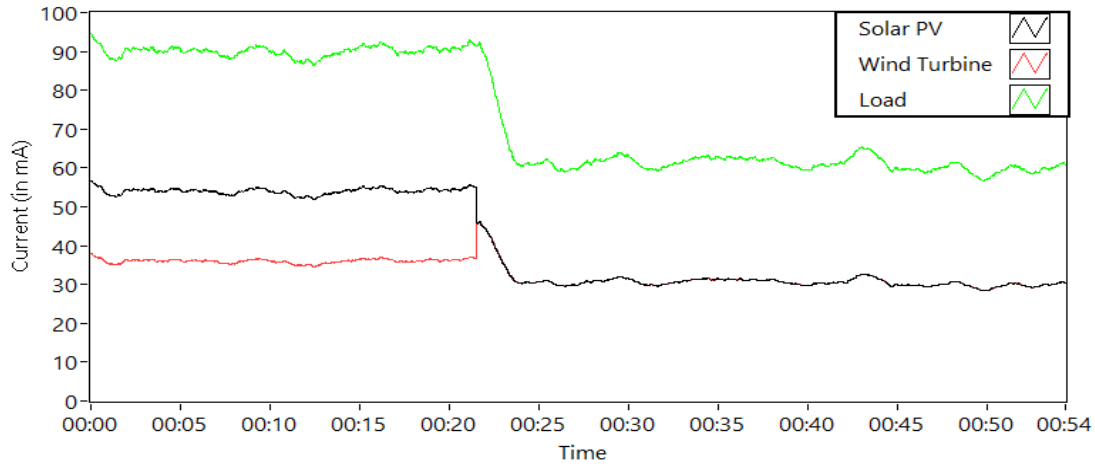

Figure 25 Experiment case 1: current response

2) Experiment case 2: Constant irradiance and variable wind speed and auto load adjustment

Fig 34 and 35 show the before and after scenario in the experiment case 2, as the algorithm is running in auto mode it can be observed that the load bank no.3 is switched off when the power from the wind turbine is reduced due to low wind speed. It can also be observed in

fig 35 that the share of PV power increases and is generating the total power demand by the load,

From fig 28, the spike in the solar PV current generation occurs between time 00:15 to 00:20, this is due to current from the wind turbine reduces to zero which causes current output from the solar PV to increases to match the load demand before the PMS algorithm reduces the load.

Once the wind speed increases the again the system uses power from both the sources to match load current requirement. This can be observed in fig 28 where after the time stamp 00:40 load demands 90mA and PV and a wind turbine provides the total required current.

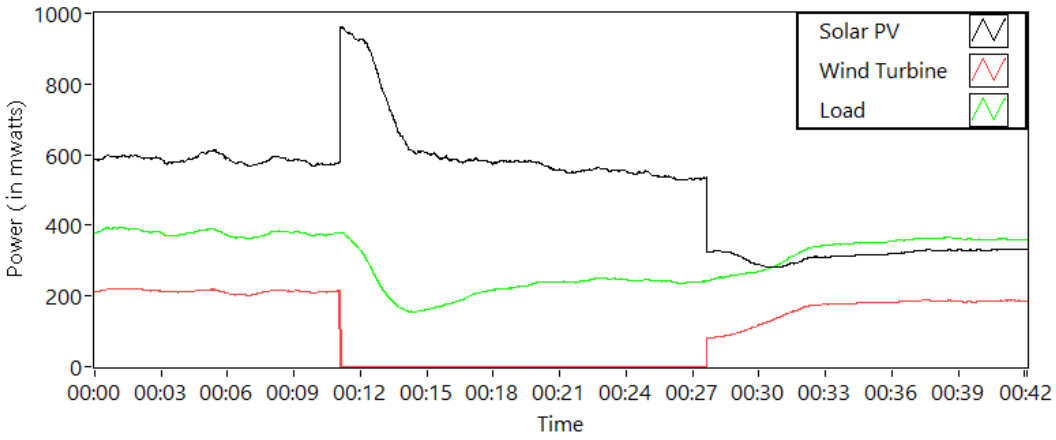

Figure 26 Experiment case 2: power response

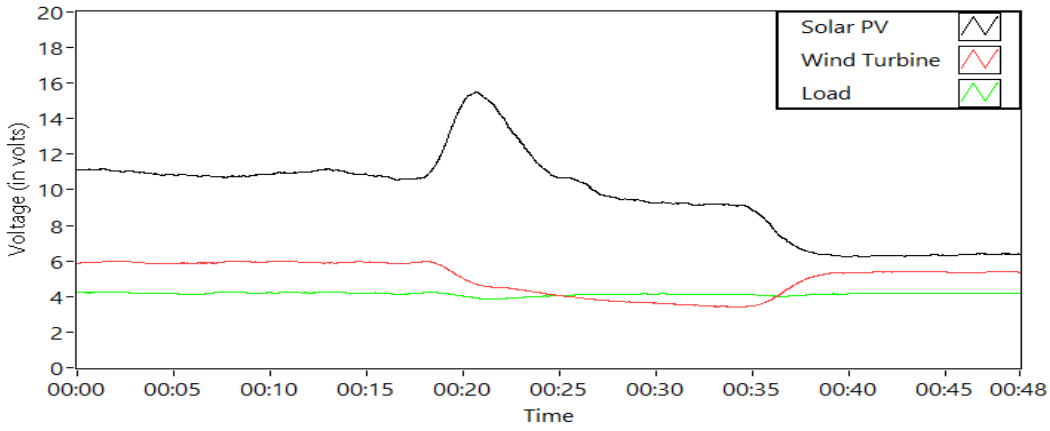

Figure 27 Experiment case 2: voltage response

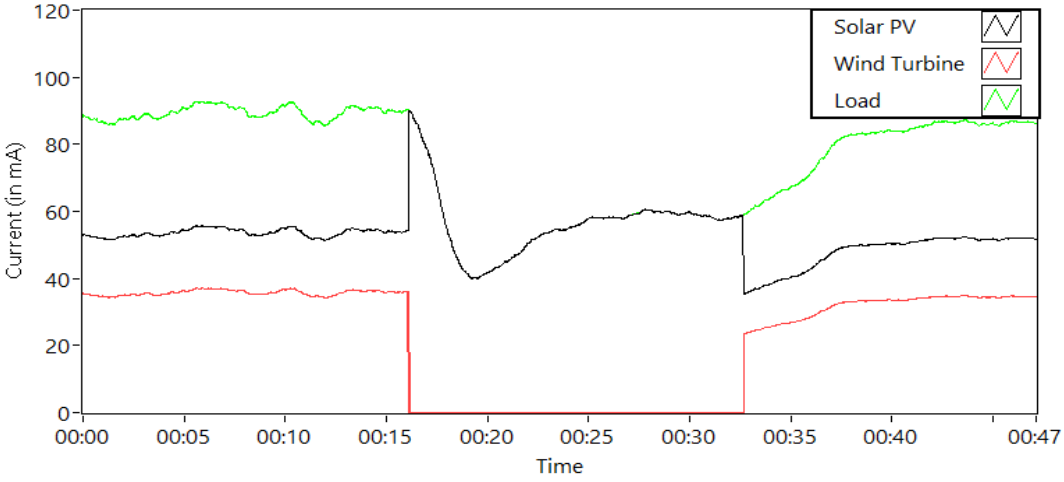

Figure 28 Experiment case 2: current response

3) Experiment case 3: Variable irradiance and wind speed and auto load adjustment

In this experiment case, fig 36 shows scenario when both the power supply provide adequate power to power all the load banks. fig 37 shows the scenario when the reduction in irradiance causes the system PMS algorithm to reduce the load and further reduction in

wind speed causes the power output to reduce even further, which triggers the reduction in load as seen in fig 38.

Form power response was seen in fig 31 it can be observed the similar phenomenon as mentioned in previous cases, about the current compensation by other power supply in case the any one of them reduce the power output due to variable weather conditions.

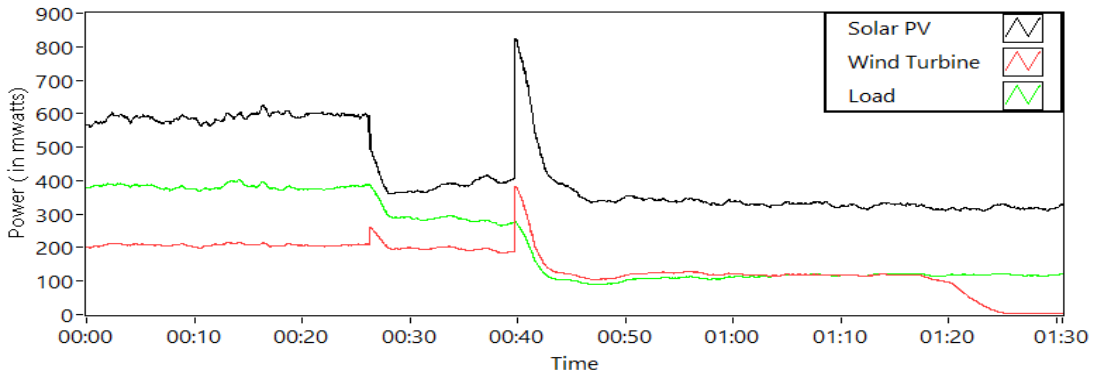

Figure 29 Experiment case 3: power response

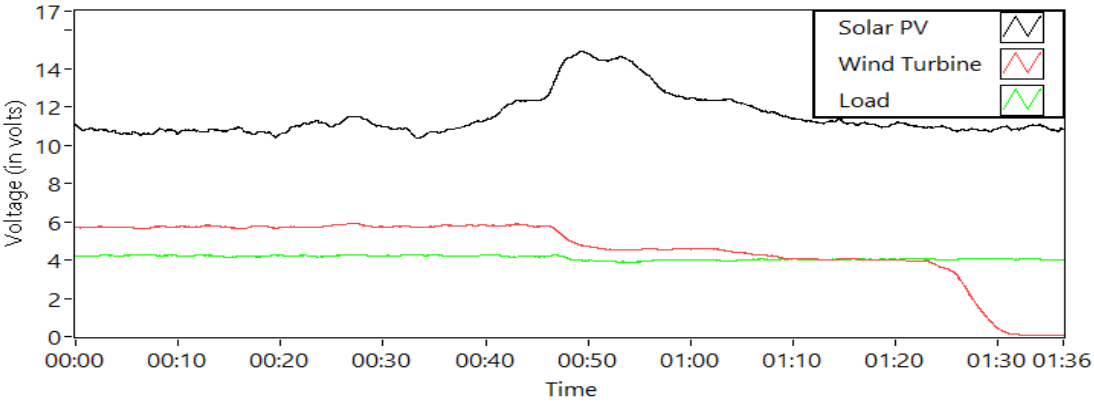

Figure 30 Experiment case 3: voltage response

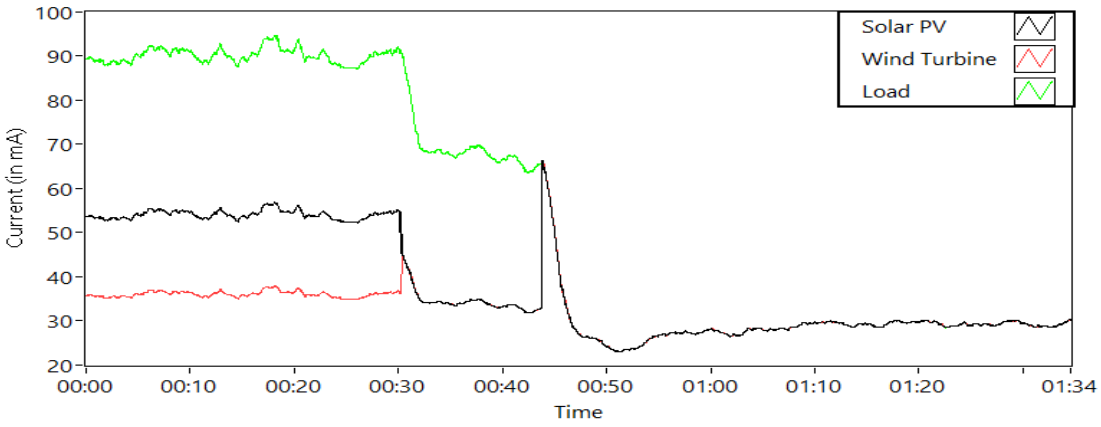

Figure 31 Experiment case 3: current response

4) Experiment case 4: Variable wind speed and irradiance and Manual load adjustment

In this experiment case user get the option to set the load priority and this manual mode checks the power from both the power generating sources and prompts the user in case the load demand cannot be met by the supply side.

Fig 39 shows the scenario when the single load bank is supplied power with the only the solar PV as a source, here user does not get the prompt to reduce the load since supply and demand match in this case. In fig 40 power from a wind turbine is introduced as the wind speed increase above turbine cut-off speed. In this scenario also, the user does not receive any prompts since the user has not increased the load. In fig 41 the user gets the prompt to the load due to low power from both the solar PV and wind turbine is unable to match the load demand.

Chapter 7 Conclusion and Recommendation

Conclusion

As the distributed generation increases across the world due to a reduction in renewable energy cost, more of these generation sources will seek grid integration and work as an islanded microgrids. In such situations, power management will be imperative to all these microgrids to better use the energy installation to achieve good value by optimized usage. Power management system designed in this work can give a basic building block to build the similar, more complex system with grid implementation. Power management system in future Smart grids is the core component which can use weather forecasting and load scheduling to better optimize the power usage and use excess power to either sell back to the grid or store in the battery storage for eventual use. The supervisory control user interface designed in this work can be used as a tool for research and education and test various power management algorithms.

Suggestions for Future Work

Control strategy for this power management system can be developed with the addition of more scenarios to make it more robust in all possible situations faced by the power grid.

In this research project, the system was designed without the storage and hence excess power was either dissipated or maximum power was not extracted from the renewable energy sources hence, the addition of energy storage device (battery) or fuel cell can be done for the well-optimized system.

The control loops designed in this work use PI controller, which can be replaced by other robust and better controllers to improve the system response.

Based on similar lines a high-power prototype microgrid can be developed which will be an exciting and challenging research topic to work on.

Appendix

Front panel interface for various experiment cases.

1. Experiment case 1: Variable Irradiance and constant wind speed and auto load adjustment.

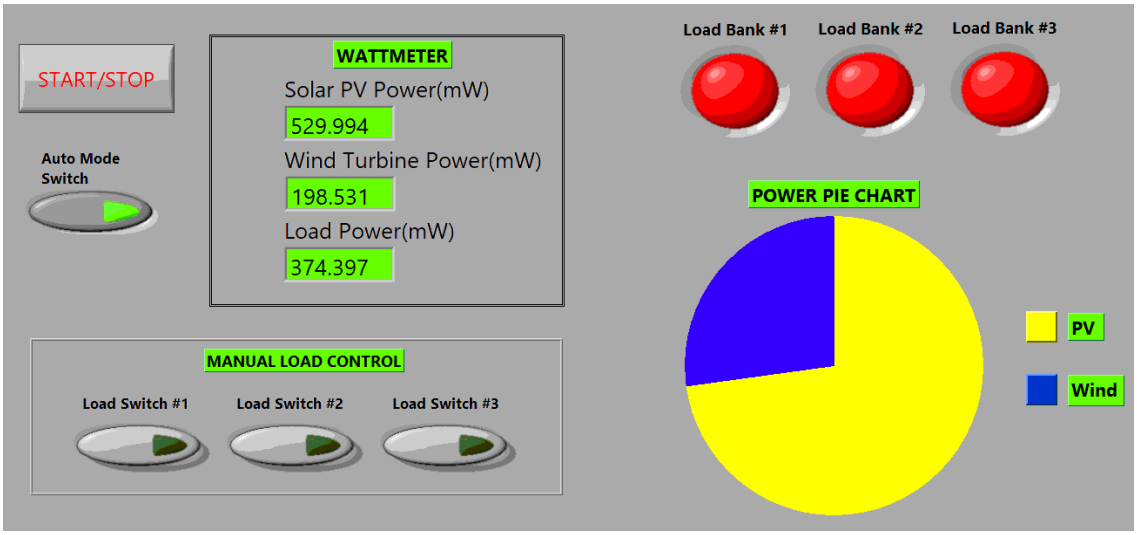

Figure 32 Front panel during constant irradiance

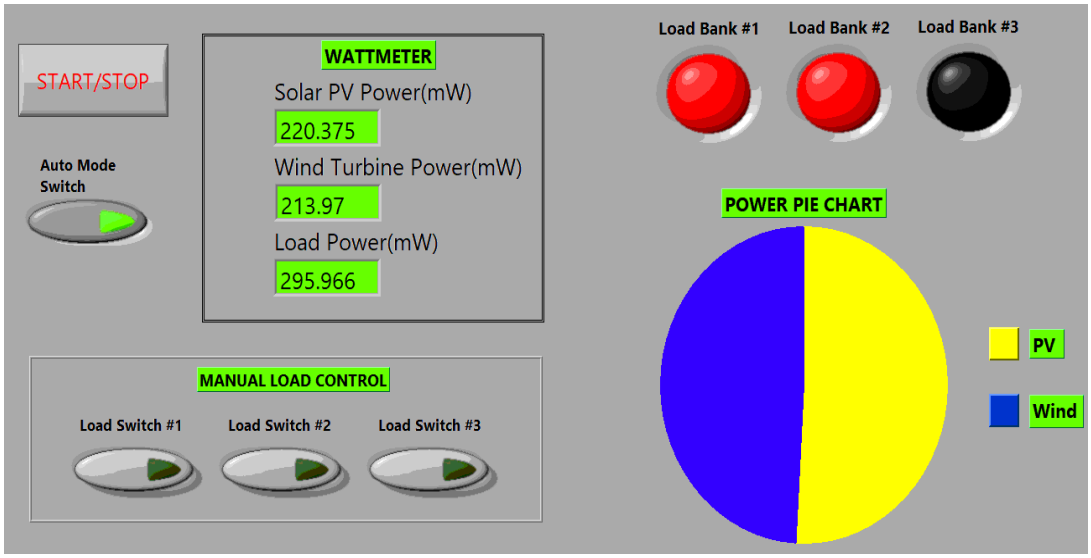

Figure 33 Front panel during variable irradiance

2. Experiment case 2: Constant irradiance and variable wind speed and auto load adjustment

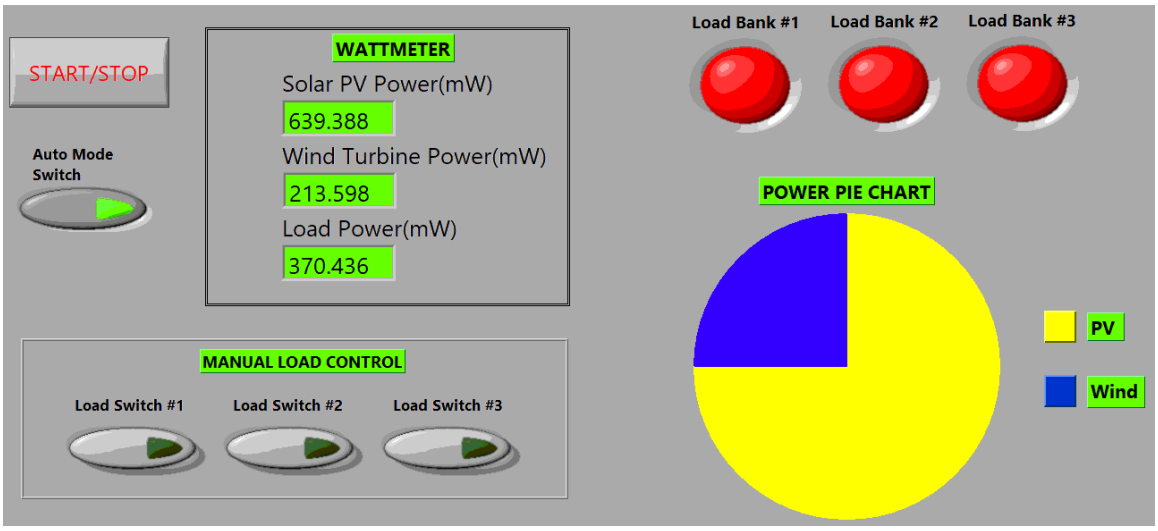

Figure 34 Front panel during constant wind speed

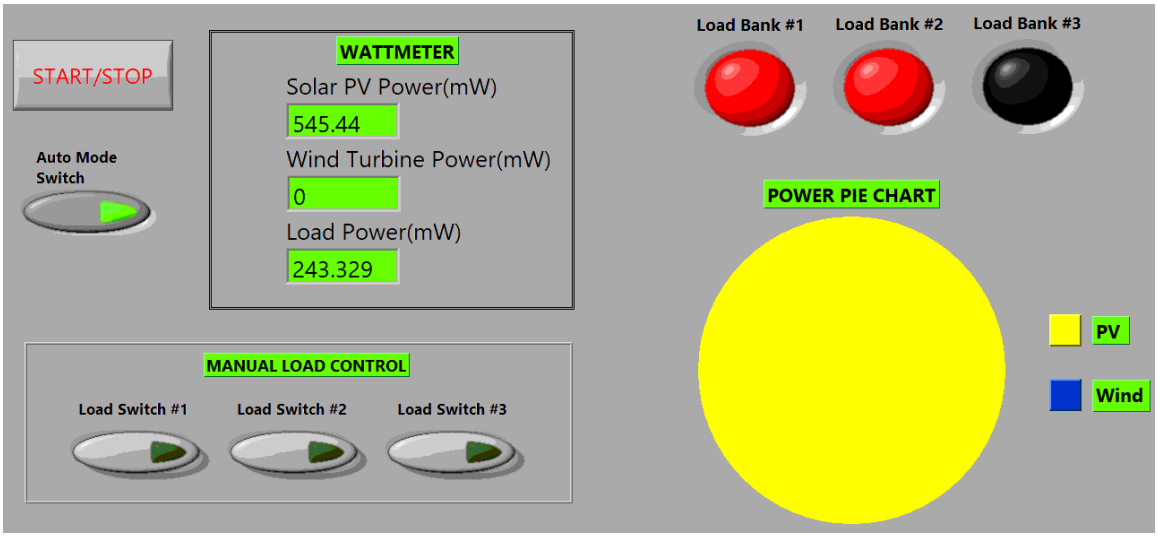

Figure 35 Front panel during variable wind speed

3. Experiment case 3: Variable irradiance and wind speed and Auto Load adjustment

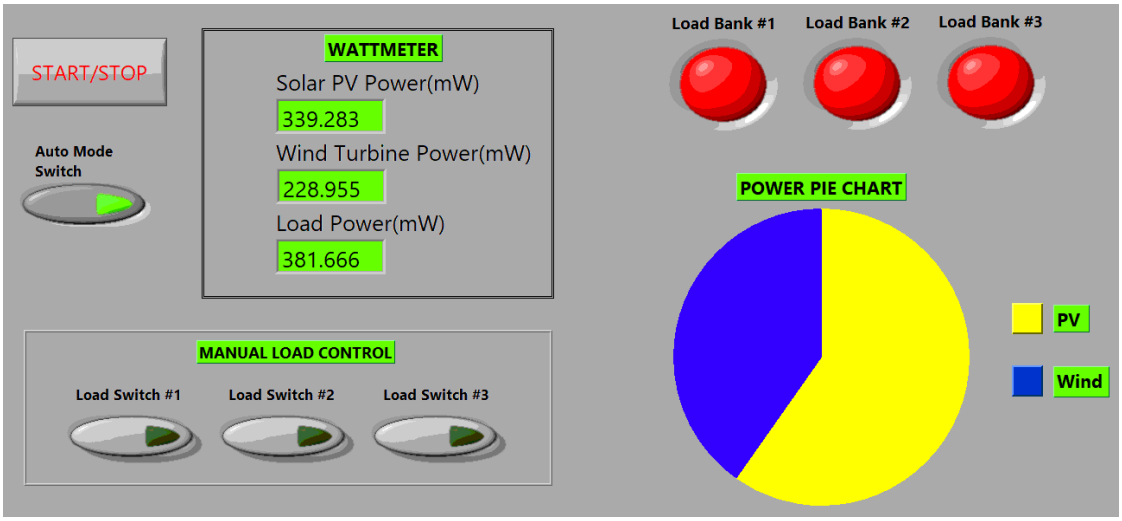

Figure 36 Front panel during constant irradiance and wind speed

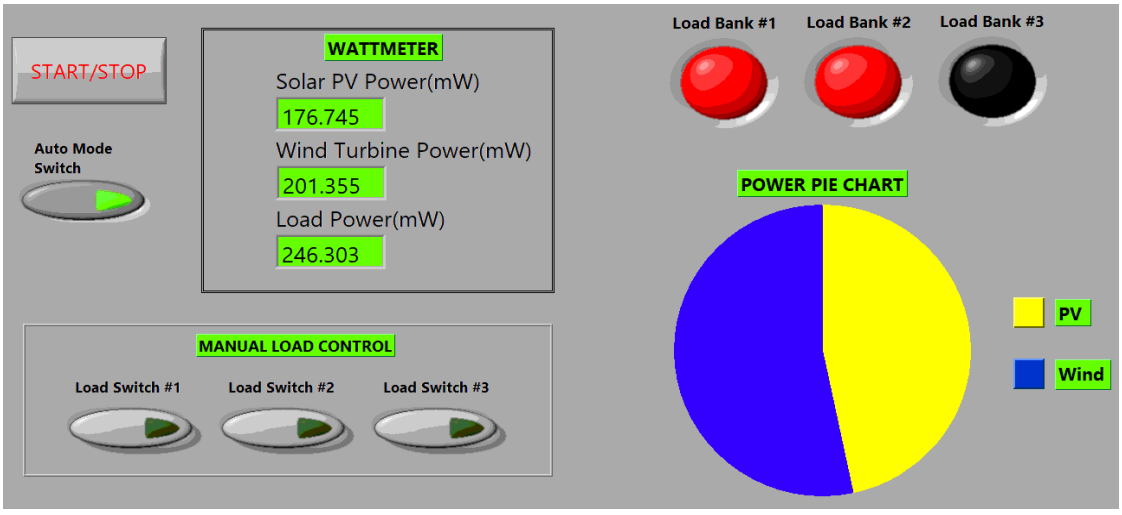

Figure 37 Front panel during variable irradiance and constant wind speed

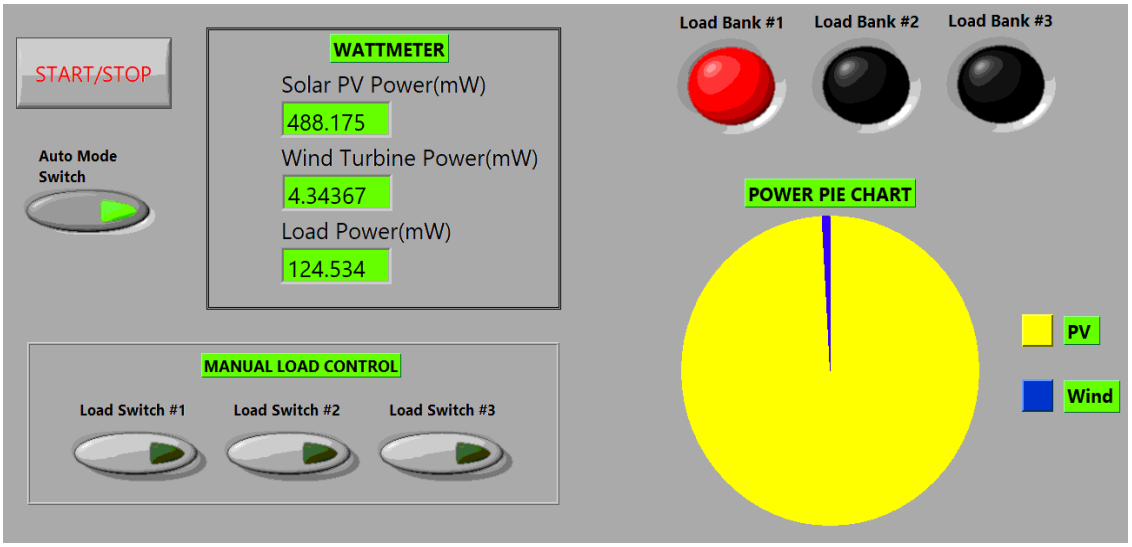

Figure 38 Front panel during variable irradiance and wind speed

4. Experiment case 4: Variable wind speed and irradiance and Manual load adjustment

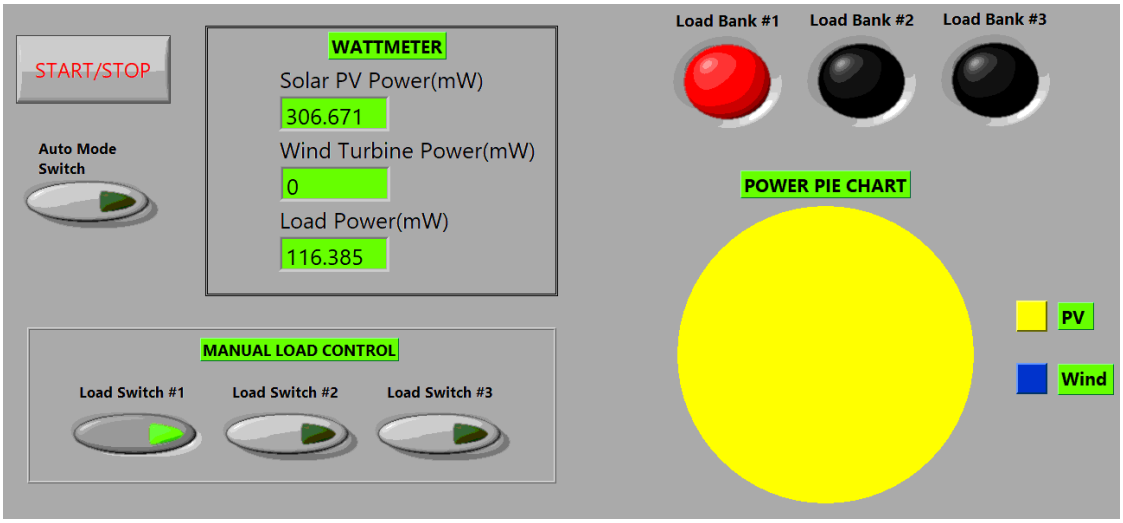

Figure 39 Front panel during sufficient power supply to the load

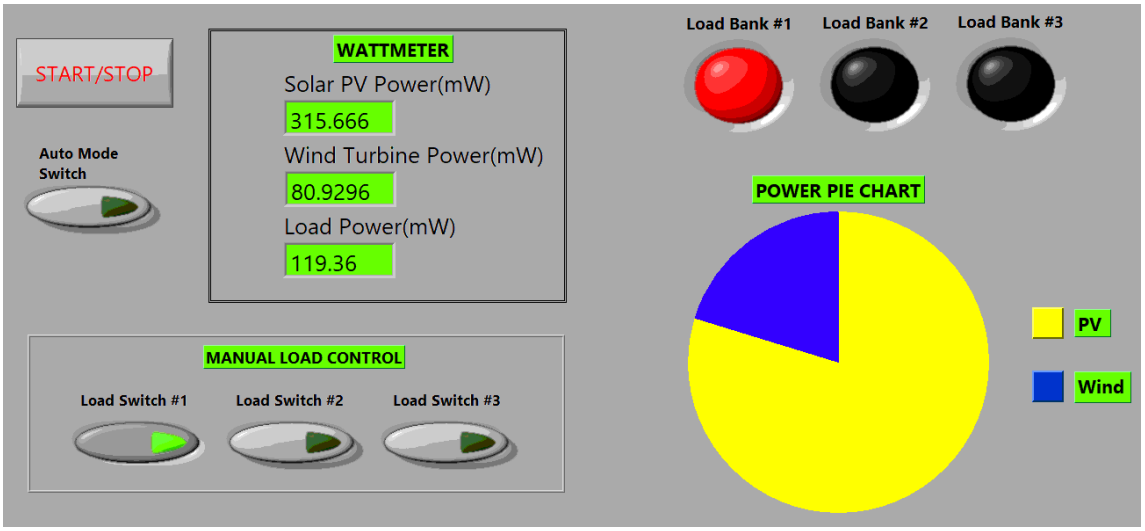

Figure 40 Front panel during surplus power supply to the load

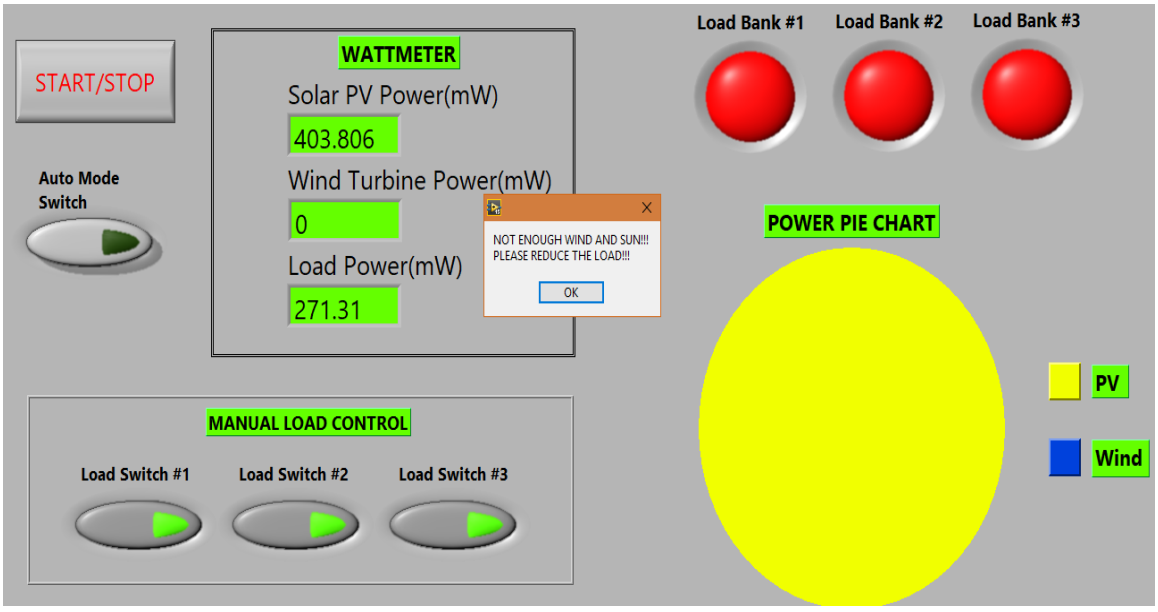

Figure 41 Front panel during low power supply to the load

References

[1] Our Electricity Future: Nova Scotia's Electricity Plan http://energy.novascotia.ca/sites/default/files/files/FINAL%20Our%20Electricity%20Future(1).pdf

[2] K. T. Ahmed, A. Merabet, H. Ibrahim, R. Beguenane, (2016), Standalone Wind Energy Conversion System Using OPAL-RT Real-time HIL/RCP Laboratory, *2nd IEEE International Conference on Industrial Informatics and Computer Systems*, Mar. 13-15, Sharjah, UAE, pp. 1-5.

[3] A. Merabet, Md. A. Islam, R. Beguenane, H. Ibrahim (2014). Second-order sliding mode control for variable speed wind turbine experiment system, Renewable Energy & Power Quality Journal, vol. 12, pp. 1-6.

[4] A. Merabet, Md. A. Islam, R. Beguenane (2014). Predictive speed controller for laboratory size wind turbine experiment system, *Canadian Conference on Electrical and Computer Engineering*, Toronto, ON, Canada, May 4-7, pp. 1-6.

[5] C. Evangelista, F. Valenciaga and P. Puleston, "Multivariable 2-sliding mode control for a wind energy system based on a double-fed induction generator", *International Journal of Hydrogen energy* 37, 2012, pp. 10070–10075.

[6] H. Amimeur, D. Aouzellag, R. Abdessemed and K. Ghedamsi. "Sliding mode control of a dual-stator induction generator for wind energy conversion systems*", Electrical Power and Energy Systems,* 42, 2012, pp. 60-70.

[7] A. A Tanvir, A Merabet, R Beguenane (2015). Real-time control of active and reactive power for doubly fed induction generator (DFIG)-based wind energy conversion system, Energies, vol. 8, no. 9, pp. 10389-10408.

[8] C. Evangelista, P. Puleston and F. Valenciaga, "Wind turbine efficiency optimization. Comparative study of controllers based on second order sliding modes", International Journal of Hydrogen Energy, 35, 2010, pp. 5934 – 5939.

[9] B. Beltran, T. Ahmed-Ali and M. El Hachemi Benbouzid, "High Order Sliding Mode Variable-Speed Wind Energy Turbines*", IEEE Transactions on Energy Conversion, vol. 56*, no. 9, pp. 3314-3321, 2009.

[10] A Merabet, K.T. Ahmed, H. Ibrahim, R. Beguenane (2016). Implementation of sliding mode control system for generator and grid sides control of wind energy conversion system, IEEE Transactions on Sustainable Energy, vol. 7, no. 3, pp. 1327-1335.8.

[11] A. Merabet, J. Kerr, V. Rajasekaran and D. Wight, "Power Electronics Circuit for Speed Control of Experimental Wind Turbine," in *24th International Conference of Microelectronics*, December 17-20, 2012, Algiers, Algeria.

[12] A. Merabet, M. A. Islam, R. Beguenane, A. M. Trzynadlowski (2015) Multivariable control algorithm for laboratory experiments in wind energy conversion, Renewable Energy, vol. 83, pp. 162-170.

[13] S. Mekhilef, R. Saidur and A. Safari, "A review on solar energy use in industries," *Renewable and Sustainable Energy Reviews*, vol. 15, no. 4, pp. 1777-1790, may 2011.

[14] K.H. Solangi, M.R. Islam, R. Saidur, N.A. Rahim and H. Fayaz, "A review on global solar energy policy," *Renewable and Sustainable Energy Reviews*, vol. 15, no. 4, pp. 2149-2163, may 2011.

[15] M.A. Eltawil and Z. Zhao, "Grid-connected photovoltaic power systems: Technical and potential problems ”A review," *Renewable and Sustainable Energy Reviews*, vol. 14, no. 1, pp. 112-129, Jan 2010.

[16] M.A.G. de Brito, L.P. Sampaio, L.G. Junior and C.A. Canesin, "Research on photovoltaics: Review, trends and perspectives," in *Power Electronics Conference (COBEP), 2011 Brazilian*, 2011, pp. 531-537.

[17] R. Rajesh and Carolin Mabel M., "A comprehensive review of photovoltaic systems," *Renewable and Sustainable Energy Reviews*, vol. 51, pp. 231-248, nov 2015.

[18] T. Esram, P.L. Chapman, "Comparison of Photovoltaic Array Maximum Power Point Tracking Techniques," *IEEE Transactions on Energy Conversion*, vol. 22, no. 2, pp. 439-449, June 2007.

[19] G.K. Singh, "Solar power generation by PV (photovoltaic) technology: A review," *Energy*, vol. 53, pp. 1-13, may 2013.

[20] T. Markvart, *Solar electricity*, Wiley, 2000, p. 280.

[21] D. Verma, S. Nema, A.M. Shandilya and S.K. Dash, "Maximum power point tracking (MPPT) techniques: Recapitulation in solar photovoltaic systems," *Renewable and Sustainable Energy Reviews*, vol. 54, pp. 1018-1034, Feb 2016.

[22] Md. A. Islam, A. Merabet, R. Beguenane and H. Ibrahim (2013) Modeling solar photovoltaic cell and simulated performance analysis of a 250W PV module, *IEEEElectrical Power and Energy Conference*, Halifax, Canada, August 21-23, pp. 1-6.

[23] S. Yang, "Solar energy control system design," 2013.

[24] B. Subudhi and R. Pradhan, "A comparative study on maximum power point tracking techniques for photovoltaic power systems," *Sustainable Energy, IEEE Transactions on*, vol. 4, no. 1, pp. 89-98 2013.

[25] a. Mellit, H. Rezzouk, a. Messai and B. Medjahed, "FPGA-based real-time implementation of MPPT-controller for photovoltaic systems," *Renewable Energy*, vol. 36, no. 5, pp. 1652-1661 2011.

[26] E. Koutroulis, K. Kalaitzakis and V. Tzitzilonis, "Development of an FPGA-based system for real-time simulation of photovoltaic modules," in *Microelectronics Journal*, 2009, pp. 1094-1102.

[27] P. A. Lynn, *Electricity from Sunlight: An Introduction to Photovoltaics*, John Wiley & Sons, 2010, p. 238.

[28] Md. A. Islam, A. Merabet, R. Beguenane, H. Ibrahim, H. Ahmed (2014). Simulation-based study of maximum power point tracking and frequency regulation for stand-alone solar photovoltaic systems, Renewable Energy & Power Quality Journal, vol. 12, pp.1-6.

[29] A. Chouder, S. Silvestre, B. Taghezouit and E. Karatepe, "Monitoring, modelling and simulation of PV systems using LabVIEW," *Solar Energy*, vol. 91, pp. 337-349, may 2013.

[30] A. Merabet, L. Labib, A. M. Y. M. Ghias, C. Ghenai, T. Salameh (2017). Robust feedback linearizing control with sliding mode compensation for a grid-connected photovoltaic inverter system under unbalanced grid voltages, IEEE Journal of Photovoltaics, vol. 7, no. 3, pp. 828-838.

[31] Camacho, Eduardo F., et al. "Control for renewable energy and smart grids."The Impact of Control Technology", *Control Systems Society* (2011): 69-88.

[32] S. Sinha and S.S. Chandel, "Review of recent trends in optimization techniques for solar photovoltaic "wind-based hybrid energy systems," *Renewable and Sustainable Energy Reviews*, vol. 50, pp. 755-769, Oct 2015.

[33] Blaabjerg, R. Teodorescu, M. Liserre and A.V. Timbus, "Overview of control and grid synchronization for distributed power generation systems," *IEEE Trans.Ind.Electron.*, vol. 53, no. 5, pp. 1398-1409, OCT 2006.

[34] Md. A. Islam, A. Merabet, R. Beguenane and H. Ibrahim (2014). Power management strategy for solar stand-alone hybrid energy system, International Journal of Electrical, Robotics, Electronics and Communications Engineering, vol. 8, no. 6, pp. 783-787.

[35] A. Buccella, C. Cecati and H. Latafat, "Digital control of power Converters—A survey," *Industrial Informatics, IEEE Transactions on*, vol. 8, no. 3, pp. 437-447 2012.

[36] E.T. Mekonnen, J. Katcha and M. Parker, "An FPGA-based digital control development method for power electronics," in *IECON 2012 - 38th Annual Conference on IEEE Industrial Electronics Society*, 2012, pp. 222-226.

[37] J. Rocabert, A. Luna, F. Blaabjerg and P. Rodriguez, "Control of power converters in AC microgrids," in *IEEE Transactions on Power Electronics*, 2012, pp. 4734-4749.

[38] U. Sadek, Sarjavs Andrej, R. Svevcko and A. Chowdhury, "FPGA-based control of a DC-DC boost converter," *IFAC-PapersOnLine*, vol. 48, no. 10, pp. 22-27 2015.

[39] Xue Wendong, Li Po, Wang Zhi, Zhong Qiang and Hong Yongqiang, "Current predictive control for three-phase voltage source inverter based on Labview FPGA module," in *Control Conference (CCC), 2012 31st Chinese*, 2012, pp. 4250-4255.

[40] A. Izadian, G. Edelman and S. Jolnson, "Gate driver of DC-DC boost converters using national instruments LabVIEW and NImyDAQ," in *Electro/Information Technology (EIT), 2014 IEEE International Conference on*, 2014, pp. 530-532.

[41] Kaur, J. Kaushal and P. Basak, "A review on microgrid central controller," *Renewable and Sustainable Energy Reviews*, vol. 55, pp. 338-345, Mar 2016.

[42] M.T. Özdemir, M. Sönmez and A. Akbal, "Development of FPGA based power flow monitoring system in a microgrid," *Int J Hydrogen Energy*, vol. 39, no. 16, pp. 8596-8603 2014.

[43] M. Cirstea and A. Parera-Ruiz, "An FPGA controller for a combined solar / Wind power system," in *Optimization of Electrical and Electronic Equipment (OPTIM), 2010 12th International Conference on*, 2010, pp. 1103-1108.

[44] A. Merabet, K. T. Ahmed, H. Ibrahim, R. Beguenane; A. M. Y. M. Ghias (2017). Energy management and control system for laboratory scale microgrid based wind-PV-battery, IEEE Transactions on Sustainable Energy, vol. 8, no. 1, pp. 145-154.

[45] A. Merabet, R. Keeble, V. Rajasekaran, R. Beguenane, H. Ibrahim, J. S. Thongam (2012), Power management system for load banks supplied by pitch controlled wind turbine system, Applied Sciences, Special issue: Renewable Energy, vol. 2, no. 4. pp. 801-815

[46] K. T. Ahmed, A. Merabet, R. Beguenane, H. Ibrahim, A. Allagui (2016), Real-Time Platform for Controlling DC Microgrid based Standalone Solar Energy Conversion System, *2nd IEEE International Conference on Industrial Informatics and Computer Systems*, Mar. 13-15, Sharjah, UAE, pp. 1-5.

[47] Colak, S. Sagiroglu, G. Fulli, M. Yesilbudak and C. Covrig, "A survey on the critical issues in smart grid technologies," *Renewable and Sustainable Energy Reviews*, vol. 54, pp. 396-405, 2 2016.

[48] M. Soshinskaya, W.H.J. Crijns-Graus, J.M. Guerrero and J.C. Vasquez, "Microgrids: Experiences, barriers and success factors," *Renewable and Sustainable Energy Reviews*, vol. 40, pp. 659-672, dec 2014.

[49] P. Siano, "Demand response and smart grids ”A survey," *Renewable and Sustainable Energy Reviews*, vol. 30, pp. 461-478, Feb 2014.

[50] EI-Kanj Baitie Hania and T. Selmi, "Review of Smart Grid Systems' Requirements," in *Ecological Vehicles and Renewable Energies (EVER), 2015 Tenth International Conference on*, 2015, pp. 1-6.

[51] NI cRIO 9024 controller http://www.ni.com/en-ca/support/model.crio-9024.html

[52] Quanser Inc Q1-cRIO module https://www.quanser.com/products/q1-crio-module/

[53] National Instruments NI 9201 module http://www.ni.com/en-ca/support/model.ni-9201.html

[54] National Instruments NI 9401 module http://www.ni.com/en-ca/support/model.ni-9401.html